CHALMERS
UNIVERSITY OF TECHNOLOGY

Ecophon
SAINT-GOBAIN

CHALMERS
UNIVERSITY OF TECHNOLOGY

Recycling of glass wool waste by geopolymerization

Master's thesis in Materials Chemistry

JENNIFER VON

DEPARTMENT OF CHEMISTRY AND CHEMICAL ENGINEERING
CHALMERS UNIVERSITY OF TECHNOLOGY

Gothenburg, Sweden 2022
www.chalmers.se

Master's thesis 2022

Recycling of glass wool waste by geopolymerization

JENNIFER VON

CHALMERS
UNIVERSITY OF TECHNOLOGY

Department of Chemistry and Chemical Engineering
Chalmers University of Technology
Gothenburg, Sweden 2022

Recycling of glass wool waste by geopolymerization
JENNIFER VON

© JENNIFER VON, 2022.

In collaboration with Saint-Gobain Ecophon
Supervisor: Saleh Hooshmand, Saint-Gobain Ecophon
Supervisor: Arezou Baba Ahmadi, Chalmers University of Technology, Department of Architecture and Civil Engineering, Building Technology, Building Materials
Examiner: Luping Tang, Chalmers University of Technology, Department of Architecture and Civil Engineering, Building Technology, Building Materials

Master's Thesis 2022
Department of Chemistry and Chemical Engineering
Chalmers University of Technology
SE-412 96 Gothenburg
Telephone +46 31 772 1000

Cover: Logo Saint-Gobain Ecophon (left), logo Chalmers University of Technology (right)

Printed by Chalmers Reproservice
Gothenburg, Sweden 2022

Recycling of glass wool waste by geopolymerization
JENNIFER VON
Department of Chemistry and Chemical Engineering
Chalmers University of Technology

Abstract

The master thesis project is in collaboration with Saint-Gobain Ecophon. This project is in relation to the WOOL2LOOP project (part of the EU Horizon 2020) with the aim of minimizing mineral wool waste by incorporating it into novel and existing products. This master thesis examines the possibilities of using glass wool waste as the main precursor to produce cementitious materials. Different mix compositions including different glass wool contents and the addition of two types of slag from steel industries were investigated. Process parameters including curing temperature and curing time have been studied to reduce future manufacturing costs. Precursor and additional slag were mixed with water glass and cured in an oven and/or at the room temperature. The cementitious materials' performance was evaluated by measuring the compressive strength after 7 and 28 days. The phase compositions were analyzed using XRD (X-ray diffraction) and TGA (Thermogravimetric analysis) respectively to better understand the mechanical strength.

The results show that glass wool, in combination with other additives, is a promising precursor for manufacturing cementitious materials. N-A-S-H and C-(N)-A-S-H have been observed in certain compositions which explains the lower strength. The materials formed through the use of lower processing temperatures have displayed good strength development with time, and a curing time of 24 h has shown high strength. Although, a curing time of 4 h has resulted in comparable strength. Further, high strength has also been achieved by curing at the room temperature.

Keywords: geopolymers, alkali-activated materials, mineral wool, recycling

Sammanfattning

Detta examensarbete har varit i samarbete med Saint-Gobain Ecophon. Projekt är en del av det EU-finansierade WOOL2LOOP projektet (en del av EU Horizon 2020) med målet att minimera avfall bestående av mineralull. Detta examensarbete undersöker möjligheten att använda glasull för tillverkning av cementlikande material. Prover med olika kompositioner inklusive olika andelar av glasull samt tillägg av slag från stålindustrin har undersökts. Processparametrar inklusive härdningstemperatur och -tid har studerats med målet att minska framtida produktionskostnader. Utvärdering av materialen utfördes genom att mäta deras tryckhållfasthet efter 7 respektive 28 dygn efter härdning. Materials faskompositioner undersöktes med XRD (X-ray diffraktion) och TGA (Termogravimetrisk analys) för att få en bättre förståelse för deras hållfasthet.

Från resultaten framgår det att glasull, i kombination med andra additiv kan utgöra ett bra utgångsmaterial för tillverkning av cementlikande material. N-A-S-H och C-(N)-A-S-H har observerats i vissa kompositioner vilket förklarar den lägre tryckhållfastheten hos materialen. Lägre härdningstemperaturer har resulterat i god utveckling i hållfasthet över tid. Längre härdningstider har också resulterat i högre hållfasthet, däremot har även kortare härdning resulterat i jämförbart resultat efter 28 dygn. Dessutom har härdning i rumstemperaturen även givit goda resultat.

Nyckelord: geopolymerer, alkali-aktiverade material, mineralull, återvinning

Acknowledgments

Big thanks to everybody at the R&D department at Saint-Gobain Ecophon who has helped me with this thesis. I would like to especially thank my supervisor Saleh Hooshmand for not only giving guidance and insight into the world of research, but also showing me the place where I could find the best coffee at Ecophon. Also, a big thank you to Craig Simkiss for supporting the technical aspects of the TGA measurements. I would also like to thank Johan Borgström and Axel Rüther for letting me carpool with them to and from Ecophon.

Thank you to my Chalmers supervisor Arezou Baba Ahmadi for showing enthusiasm and support, and for enabling analytical measurements at the university. I would also like to thank my examiner Luping Tang for always being available to answer questions.

Lastly, thank you to Oscar Enander for bouncing ideas with me throughout these 6 months.

Jennifer Von, Gothenburg, May 31, 2022

Contents

List of abbreviations and Important Concepts ..... **xii**

List of Figures ..... **xiii**

List of Tables ..... **xv**

1 Introduction **1**

1.1 Saint-Gobain Ecophon *1*

1.2 Scope and objective *1*

1.3 Limitations *1*

2 Theory **3**

2.1 Cement and concrete *3*

2.2 Ordinary Portland Cement (OPC) *3*

2.3 Geopolymers *4*

2.3.1 Geopolymerization 5

2.3.2 Geopolymers vs alkali activated materials 9

2.4 Precursors *9*

2.4.1 Glass wool (GW) 9

2.4.2 Metakaolin 11

2.4.3 Other precursors and additives 12

2.4.4 Ratios 13

2.5 Alkali reagents *13*

2.5.1 Sodium hydroxide (NaOH) and potassium hydroxide (KOH) 13

2.5.2 Alkali-silicates (K, Na-Si_xO_y) – Water glass 14

2.6 Curing temperature and curing time *14*

Phases in geopolymers and AAM *15*

2.7 ..... *15*

2.7.1 N-A-S-H (Sodium aluminosilicate hydrate) and K-A-S-H (Potassium aluminosilicate hydrate) 15

2.7.2 C-S-H (calcium silicate hydrates) and C-A-S-H (Calcium aluminosilicate hydrate) and C-(N)-A-S-H 16

2.7.3 Other phases 17

2.8 Characterization *17*

2.8.1 Calorimetry 17

2.8.2 Mechanical measurement 18

2.8.3 X-ray diffraction (XRD) 19

2.8.4 Thermogravimetric analysis (TGA) 20

2.8.5 Optical microscopy 21

3 Experimental method **23**

3.1 Materials *23*

3.2 Laboratory work *23*

3.2.1 Reactivity 23

3.2.2 Wet slurry 23

3.3 Characterization *25*

3.3.1 Calorimetry measurement 25

3.3.2 Mechanical measurements 25

3.3.3 XRD 25

3.3.4 TGA 25

4 Results and Discussions 26
4.1 Calorimetry *26*
4.2 XRD *27*
4.3 TGA *28*
4.4 Curing temperature and curing time *30*
4.5 Mechanical measurements *31*
4.6 Optical microscopy *34*
5 Conclusion 35
6 Future work 36
References 37
APPENDIX A 41
APPENDIX B 45

List of abbreviations and Important Concepts

Abbreviation	English	Svenska
AAM	Alkali-Activated Materials	Alkali-aktiverade material
GP	Geopolymers	Geopolymer
MK	Metakaolin	Metakaolin
GW	Glass Wool	Glasull
w/b	Water-to-binder ratio	Vattenbindemedeltal
L/S	Liquid-to-solid ratio	Kvoten mellan vätska och fast material
OPC	Ordinary Portland Cement	Portlandcement
Ca	Calcium	Kalcium
Si	Silicon	Kisel
Al	Aluminum	Aluminium
Na	Sodium	Natrium
K	Potassium	Kalium

List of Figures

Figure 2.1. Names of units consisting of silicon, oxygen and aluminum 4
Figure 2.2. Ortho-siloxonate 5
Figure 2.3. Ortho-sialate 5
Figure 2.4. Alkalination 6
Figure 2.5. Depolymerization of silicates 6
Figure 2.6. Gel formation and oligo sialate formation 6
Figure 2.7. Polycondensation between molecules forming oligomers and larger networks 7
Figure 2.8. Further polycondensation 7
Figure 2.9. Further polycondensation and formation of albite framework 8
Figure 2.10. Relationship between chemistry and processing step. 8
Figure 2.11. Data of GW1, GW2, GW3 from "Utilization of Mineral Wools as Alkali-Activated Material Precursor" 11
Figure 2.12. Formation of (N, K)-A-S-H 15
Figure 2.13. Ternary diagram showing N-A-S-H and stoichiometric geopolymer 16
Figure 2.14. Ternary diagram showing C-A-S-H and C-(N)-A-S-H 16
Figure 2.15. Stress-strain curve showing different characteristic regions in which a material can have. [58] 18
Figure 2.16. Tensile machine for compressive strength measurements 19
Figure 2.17. Diffraction in crystal planes based on Bragg's law 19
Figure 2.18. XRD instrument with some main components marked 20
Figure 2.19. Thermogravimetric analysis instrument 20
Figure 2.20. Optical microscope 22
Figure 3.1. GW, MK, Slag2, Slag1, water glass (raw material) 23
Figure 3.2. Experimental steps 24
Figure 4.1. Reactivity of geopolymer components (raw material) 26
Figure 4.2. XRD spectra of MK S, 100% GW S, Slag2 S and Slag1 S. G-gaylussite, N-nepheline, Q-quartz, M-mullite, ASi-aluminosilicate, S-calcium sulphate, SA-sodium aluminate. 27
Figure 4.3. Ternary diagram of studied samples. 28
Figure 4.4. DTG of samples containing only GW, addition of MK, Slag2 and Slag1 respectively. 28
Figure 4.5. DTG and TGA of 100%GW S and GW raw material 29
Figure 4.6. DTG of Slag1 S and its raw materials Figure 4.7. DTG of Slag2 S and its raw materials 29
Figure 4.8. Effect of curing time and temperature on the compressive strength 30
Figure 4.9. The effect of glass wool waste on the compressive strength. 31
Figure 4.10. Effect of Slag1 on the compressive strength. Figure 4.11. Effect of Slag2 on the compressive strength 32
Figure 4.12. Stress-strain curves of samples after 7 days of curing. 32
Figure 4.13. Relation between L/S, w/b, alkali concentration and compressive strength 33
Figure 4.14. MK S (upper left), Slag2 S (upper right), Slag1 S (bottom left), 100% GW S (bottom right) 34

Figure A 1. XRD spectra of MK S 41
Figure A 2. XRD spectra of Slag2 S 41
Figure A 3. XRD spectra of 100%GW S 42
Figure A 4. XRD spectra of Slag1 S 42
Figure A 5. XRD spectra of GW raw material 43
Figure A 6. XRD spectra of Slag2 raw material 43
Figure A 7. XRD spectra of MK raw material 43
Figure A 8. XRD spectra of Slag1 raw material 44

Figure B 1. TGA of 100%GW S, 20%Slag1 S, 20%Slag2 S and MK S 45
Figure B 2. TGA and DTG of 100%GW S, 20%Slag1 S, 20%Slag2 S and MK S 45
Figure B 3. TGA and DTG of MK S and its raw materials 46
Figure B 4. TGA of Slag2 S and its raw materials 46
Figure B 5. TGA of Slag1 S and its raw materials 47

List of Tables

Table 2.1. Concrete grade and their characteristic compressive strength after 28 days 3
Table 2.2. Median composition of glass wool 10
Table 2.3. Chemical composition of metakaolin 12
Table 2.4. Calcination method and Al-coordination content 12
Table 3.1. Weight percentage of oxides in the components/raw materials 23
Table 3.2. Studied mix designs 24
Table 3.3. Studied curing temperature and time 25
Table 4.1. Relation between L/S, w/b, alkali concentration and compressive strength 30

1 Introduction

This master thesis project was done in collaboration with Saint-Gobain Ecophon. Saint-Gobain Ecophon develops, manufactures, and markets acoustic products and systems with large emphasis and consideration of environmental and sustainable aspects. More specifically, this project was in relation to the WOOL2LOOP project (part of the EU Horizon 2020). The WOOL2LOOP project aims to minimize waste and recycle mineral wool waste by incorporating it into novel and traditional products.

The generation of wastage from the construction and demolition industry is currently increasing globally and thus leads to landfilling of the waste. Not only does it result in non-environmentally friendly waste management, but also high waste management costs. The waste volume in Europe only, in 2010, was estimated to be 2.3 million tons.

Today, the amount of recycled mineral wool waste is still low due to a lack of knowledge in the field. Although, there are several research studies in the literature that indicate great potential, many industries are still in the starting phase of implementing it into their products; Saint-Gobain Ecophon is one of them. This project deals with utilizing glass wool to form geopolymers which are then suggested to be used as supplementary cementitious materials which will act as a more environmentally friendly alternative to Ordinary Portland Cement [1].

1.1 Saint-Gobain Ecophon

Saint-Gobain is one of the world's top 100 leading industry companies in construction, with a large focus on the environmental and sustainable aspects. The company manufactures and distributes both materials and services for a market that spans from transportation to infrastructure [2].

Ecophon is a part of the Saint-Gobain concern with a focus on developing, manufacturing and marketing acoustic systems, with ceiling panels being their specialty. Their clients range from hospitals, and offices to schools. Ecophon has offices in 20 countries and representations in an additional 30 more, and with the head office located in Hyllinge, Sweden [3].

1.2 Scope and objective

Using glass wool waste as the main precursor, a cementitious wet-mix product is going to be produced. The overall aim of this study is to incorporate as much recycled glass wool waste as possible into the product and subsequently determine how different additives and processing parameters may influence the properties of the formed product, focusing on the mechanical properties. The study will emphasize investigating the effect of glass wool content, additives including metakaolin, slag (Slag1, Slag2), and water. Further, processing parameters including curing time and temperature will be investigated.

1.3 Limitations

The most important property of the formed material is its compressive strength which is to be tested on 7 and 28 days after the samples have been prepared. Depending on the results of the mechanical tests, the product can be further optimized. This thesis is limited to focusing on the compressive strength of the formed materials along with its phases contributing to it. Geopolymers are of great interest as supplemental cementitious material in the industry due to their lower carbon footprint in comparison to Ordinary Portland Cement (OPC). Emphasis will not be put on comparing OPC with geopolymers, although it will be briefly mentioned and discussed to give a better understanding of binder systems.

Included in the thesis goal was to manufacture ceiling panels based on the obtained results of the geopolymers. However, due to delivery delays the investigation of panels including their fire and acoustic properties will not be a part of this thesis.

This master thesis is also in accordance with a non-disclosure agreement with Ecophon, and therefore certain mix compositions, brand names, name of slag and processing steps cannot be included in the public report.

2 Theory

This chapter presents the theory behind concepts, elements, and characterization techniques important for this project.

2.1 Cement and concrete

Concrete is a material used in construction. It consists of cement mixed with fine and coarse aggregates. Sand, gravel, and small-sized stone are commonly used as aggregates in different concretes. Cement act as binder for the aggregates and thus fill the gaps between the particles of different sizes. The smaller particles also have the tendency to contribute to filling gaps between larger particles. When mixed, the formed slurry hardens with time and forms a strong material with a characteristic strength after 28 days. The aggregates used are stronger than the cement and therefore contributes to an increase in strength.

Aggregates of different sizes give rise to different types of concrete. Fine aggregates are defined as those ranging from 0.025-6.5 mm in diameter whereas coarser aggregates ranges from 6.5-38 mm [4]. Depending on the application of the concrete, different grades are used with different characteristic compressive strengths. Concrete can be divided into three categories: ordinary concrete, standard concrete and high strength concrete, see Table 2.1. In the European denotation, the grade of the concrete is defined by M or C followed by a number defined by the mixture.

Table 2.1. Concrete grade and their characteristic compressive strength after 28 days

Group	**Grade**	**Characteristic strength after 28 days [MPa]**
Ordinary concrete	M10-M20	10-20
Standard concrete	M25-M55	25-55
High strength concrete	M60-M80	60-80

The ordinary concrete grades are mainly used for PCC (Plain cement concrete) including bedding for footing. The lower grades of standard concrete are used for RCC (Reinforced cement concrete) including foundations, beams, and slab, whereas the higher grades are used in applications including runways, concrete roads, and prestressed beams. The high strength concrete grades are applied in fields in which the construction is subjected to high compressive strength such as high rise building and coastal construction [5].

2.2 Ordinary Portland Cement (OPC)

Portland cement is a material with a binder consisting of finely grounded powder. It is manufactured from materials including limestone and clay. It makes up a system with four major oxides: calcium oxide (CaO), silicon dioxide (SiO_2), aluminum oxide (Al_2O_3) and iron oxide (Fe_2O_3). These oxides can be found in many materials including natural sources such as limestone. Therefore limestone is an excellent precursor for manufacturing cement [6]. OPC is commonly manufactured through a dry process in which the precursor is crushed into smaller sized particles before undergoing a pre-heating process where carbonates are dissociated into calcium oxide and carbon dioxide. The rest is transported to a rotary kiln where the material is heated at elevated temperatures (>1500°C). Calcium oxide reacts with elements in the mixture and forms calcium silicates and aluminates. The substances left in the kiln constitute the clinker, which is let to cool down before being mixed with gypsum and limestone before being grounded into a highly uniform powder [7] [8].

The powder mixture constitutes the Portland cement, which is further mixed with water and aggregates to form concrete. Portland cement in a mixture with water can also act as binder in other applications, including acoustic ceiling panels.

Cement, like OPC have in later years faced environmental challenges as its production is dependent on large amounts of fuel, the production emits large quantities of carbon dioxide which today has been responsible for 5% of the global anthropogenic carbon dioxide emission, and also 7% related to usage of fuel during manufacture [8].

The environmental impact of traditional cement production can be observed on three scales: global, regional and local scale, where the global scale focuses on the carbon dioxide emissions emitted during the calcination process and the carbon dioxide produced during generation of electricity needed to operate the cement plant. On a regional scale, sulfur dioxide and nitrogen oxide emissions result in acid rain and thus acidification of the environment. The emission originates from the fuel combustion in relation to the heating of rotary kiln. On a local scale, the particulates of both unburned and partially burned materials in the combustion gases are considered as hazardous waste due to their ability to cause irritation of the airways [8].

2.3 Geopolymers

Between the years 1970-1973 there were a series of fires in France, which all originated from organic plastic. This inspired Joseph Davidovits to do research on non-flammable and non-combustible plastic materials, which later developed into geopolymers (GP). Geopolymers are materials rich in silica and aluminum acting as a binder and therefore can be used to manufacture cementitious materials. They are more environmentally friendly than many other cements due to the lower carbon footprint, partly due to using waste as precursor and partly to a manufacturing process which does not emit high amounts of carbon dioxide. The requirement for the precursor is high amounts of silicon and aluminum to form the characteristic geopolymer structure, allowing a wide range of precursors to be utilized [9]. GP as a binder has shown to possess great properties, comparable to other binder systems, including physical and mechanical properties. It has proven to be suitable for multiple applications including concrete and coating material. Geopolymers are manufactured through using a pozzolanic material as precursor, and today waste materials with high silica and alumina content have become of interest to further decrease the environmental impact from the cement industry [10].

GPs are classified as a sub-group of polymers due to having the same processing steps as organic polymers. They are amorphous, inorganic components that form chains or networks of alternating aluminum (Al) and silica (Si) covalently bounded to oxygen (O). The properties of GP can vary significantly depending on the ratios and interactions of the constituting atoms. Depending on the bonds between Si, Al and O different chemical units are formed which are classified according to their Si:Al ratio, see Figure 2.1 [11].

-Si-O-Si-O-	(Si:Al=0, siloxo)
-Si-O-Al-O-	(Si:Al=1, sialate)
-Si-O-Al-O-Si-O-	(Si:Al=2, sialate-siloxo)
-Si-O-Al-O-Si-O-Si-O-	(Si:Al=3, sialate-disiloxo)
Si:Al > sialate link	

Figure 2.1. Names of units consisting of silicon, oxygen and aluminum

2.3.1 Geopolymerization

The geopolymer system contain covalent bonds where the formation of SiO_4 results from co-sharing of electrons between one silica atom and four oxygen atoms. Ortho-siloxonate molecules $(SiO_4)^{4-}$ (Figure 2.2) are formed with support from a metallic ion donor, commonly an alkali metal such as sodium (Na^+) or potassium (K^+) however, calcium (Ca^{2+}), magnesium (Mg^{2+}) or iron (Fe^{2+}) can also be found in a geopolymer system.

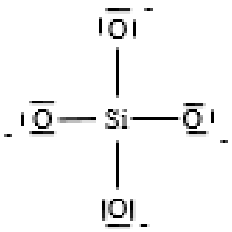

Figure 2.2. Ortho-siloxonate

Polycondensation result in formation of higher degree of siloxonate by co-sharing of electrons between Si and O. For ortho-sialate (see Figure 2.3) to form the reaction must take place in an alkaline medium.

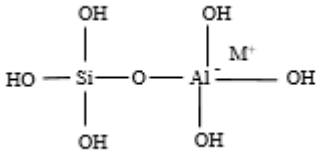

Figure 2.3. Ortho-sialate

The Al takes an electron pertaining to the alkali-metal in order to obtain a negative electrostatic charge and thus becomes tetra-valent. Subsequently the metal becomes electron deficient and thus is strongly attracted to the sialate molecule and acts as a charge balance to the negatively charged Al. The nature of the bond has long been discussed and was previously believed to be ionic. However, later research has shown that the double tetrahedron in the structure is formed through the sharing of one electron between Si and O and thus resulting in a strong covalent bond. Each Si-atom in the structure is bound to 4 O-atoms whereas each O-atom is bound to 2 Si-atoms. The atoms are not mobile in the structure, i.e., they are constrained to a position after a reaction has occurred. The difference in electronegativity results in the formation of polar covalent bonds which hold together the tetrahedral-network [12].

The geopolymerization process is carried out through reaction between oligomers of different sizes (dimer, trimer, tetramer, pentamer) and consist of the following steps: 1. alkalination, 2. depolymerization of silicates, 3. gel-formation of oligo-sialates, 4. polycondensation, 5. reticulation networking and geopolymer solidification.

During the alkalination, depolymerization of silicates and formation of oligo-sialates take place whereas the latter one is commonly known as the gel-formation. Subsequently, polycondensation take place and forms higher degrees of oligomers and additionally polymers. Depending on the cation (Na^+ or K^+), the kinetics of the polymerization may differ due to the size difference between the ions. The following section presents the reaction mechanism for the geopolymerization of metakaolin, and glass wool is assumed to have similar reaction [13].

1. Alkalination
   During the alkalination, the OH^- (oxygen hydroxide) in the alkaline medium reacts with Al pertaining the side-group of sialate which results in the formation of a tetravalent Al. The cation becomes attracted by the negatively charged Al and neutralize the region by its presence, see Figure 2.4.

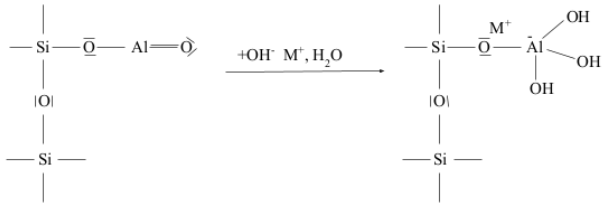

Figure 2.4. Alkalination

2. Depolymerization of silicates
   The OH^- reacts with the Si-atom which then obtains the penta-covalent state, see Figure 2.5.

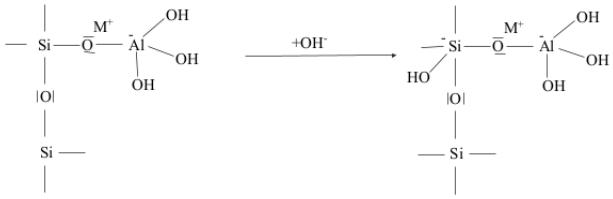

Figure 2.5. Depolymerization of silicates

3. Gel formation and oligo sialate formation
   There is cleavage of the siloxane oxygen through restructuring of electrons in the molecule, which results in the formation of silanol and siloxo, see Figure 2.6.

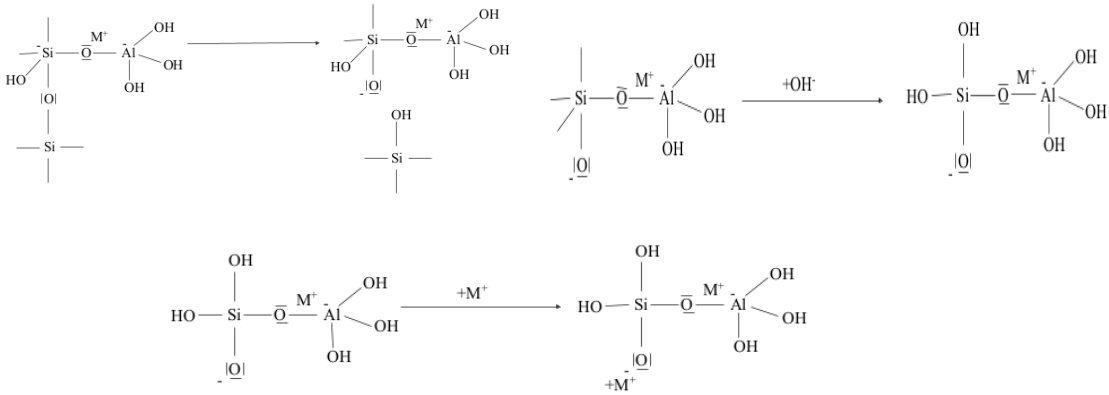

Figure 2.6. Gel formation and oligo sialate formation

There is further formation of silanol and isolation of ortho-sialate, whereas the latter one act as the primary unit in the upcoming polycondensation reaction.

Siloxo reacts with the cations and a terminal bond (-Si-O-M-) is formed, where M is the cation.

4. Polycondensation
   Reaction between ortho-sialate and aluminum oxide results in higher degree of oligomers with the metal cation being liberated from the reaction and thus acting as a catalyst in the polycondensation reaction until a large nepheline framework has been formed, see Figure 2.7.

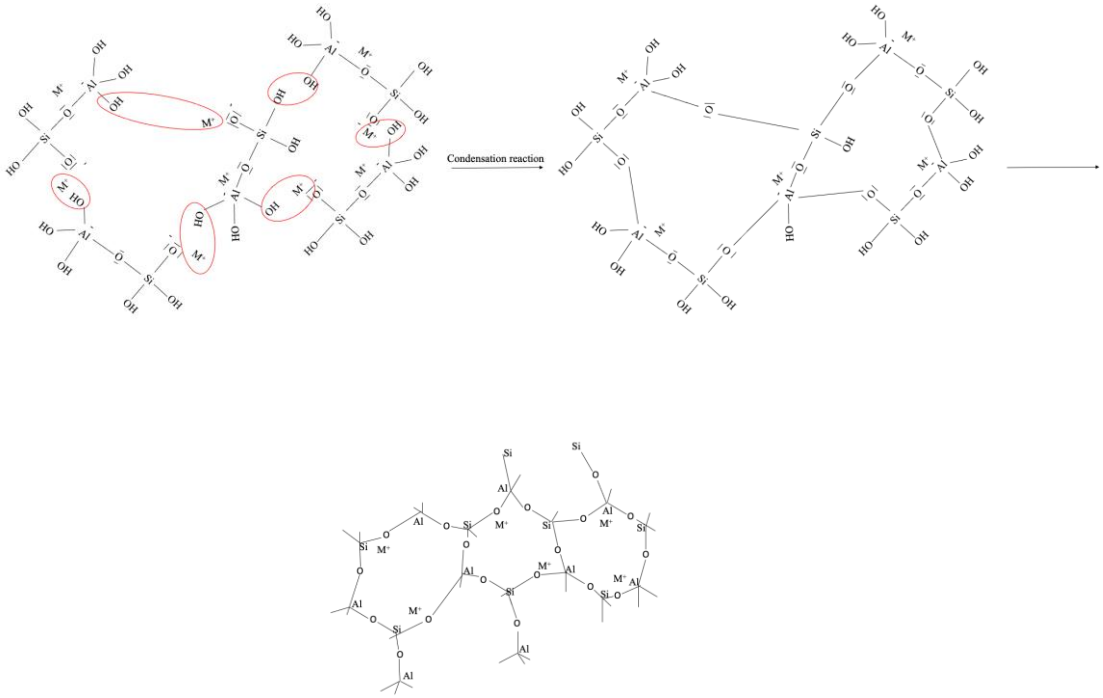

Figure 2.7. Polycondensation between molecules forming oligomers and larger networks

Further, there is condensation between di-siloxonate and ortho-sialate and the formation of a cyclic structure ortho-sialate-disiloxo in the presence of water glass. The cations are once again liberated and thus participate in further reactions, see Figure 2.8.

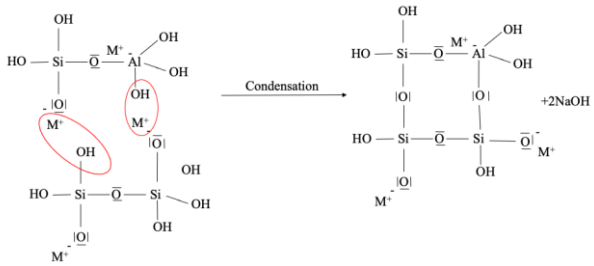

Figure 2.8. Further polycondensation

5. Polycondensation, reticulation networking and geopolymer solidification.
   Additional polycondensation results in an albite framework with its characteristic feldspar crankshaft chain structure, see Figure 2.9.

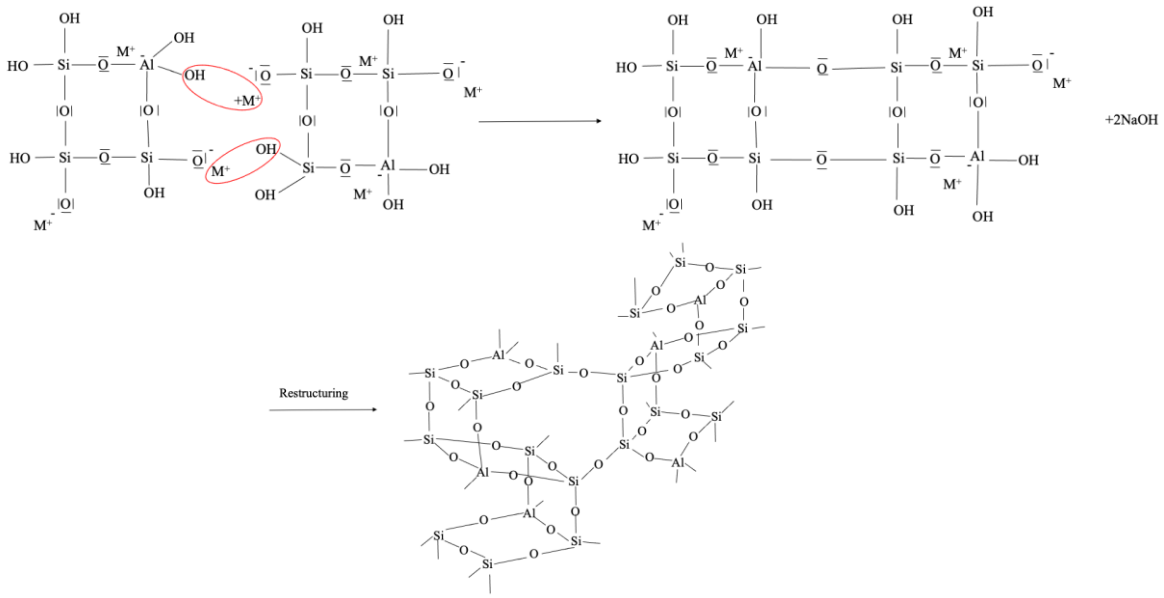

Figure 2.9. Further polycondensation and formation of albite framework

Each reaction step is related to a processing step, leading to the process and order of mixing being as essential as the chemistry. The relationship between chemistry and processing steps is presented in Figure 2.10. The hardening can be affected by appropriate curing time and temperature, and suitable casting of the mix can enable avoidance of gas bubbles. Furthermore, addition of additives and fillers can modify the final properties of the material.

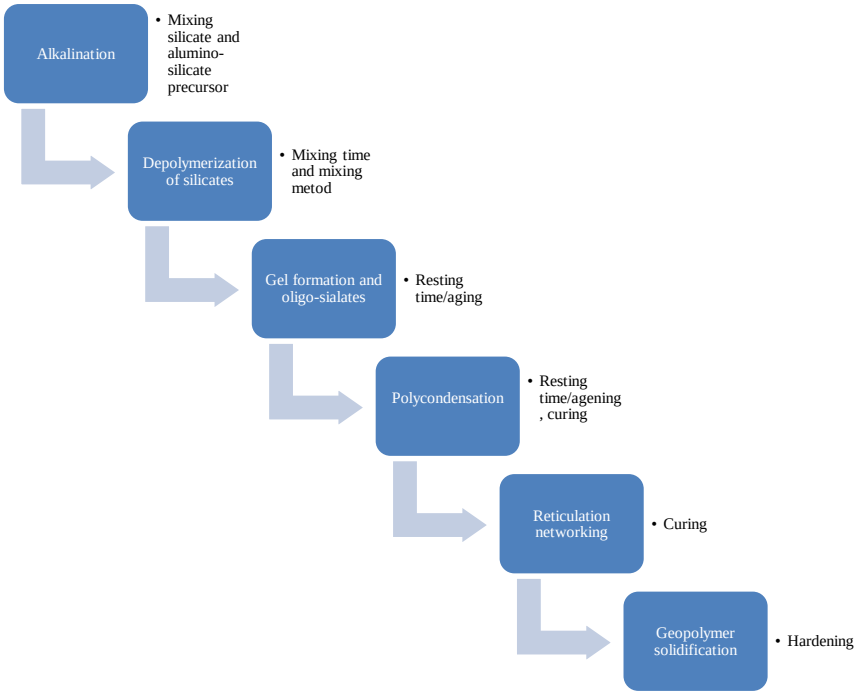

Figure 2.10. Relationship between chemistry and processing step.

2.3.2 Geopolymers vs alkali activated materials

There exists confusion between the terms geopolymer (GP) and alkali-activated material (AAM). The mistake originates from the AAM-scientists implementing GP-processing steps and thereof considering GP as a sub-group of AAM. The processing steps and order are significantly different between the two materials. The first step in geopolymerization is alkalination, which is the process of increasing the pH to above 7 by adding an alkaline medium containing potassium (K) or sodium (Na). The first processing step of AAM is alkali-activation, which is the process of activating a reaction with an otherwise inert material. GPs are polymers whereas AAM are hydrates or precipitates. Due to this, GPs and AAMs act differently upon addition of water. In GPs, water acts as transport medium for the cations during the formation of oligomers. The cations act as charge neutralizer of the negatively charged tetrahedral aluminum-centers, i.e., water is not part of the structural build-up of the network and is evaporated during the curing time. The relation between water and alkali cation content is essential as a low water-to-cation ratio (H_2O/M_2O) may cause poor transportation of the cations whereas a high ratio enables the cations to be transported from the reaction sites. The migration of cations can result in unwanted side-reactions. They can react with CO_2 in the atmosphere to form carbonates which may affect the final strength of the material. Cation deficiency on the other hand will result in not enough charge balance and thus a weaker network. Stoichiometric geopolymers result in the optimum properties as the amount of each reactant is chosen so that all is reacted during geopolymerization, i.e., there are no residual elements which can participate in unwanted reactions [13].

Even though AAMs and GPs belong to different systems, it is still possible to make a geopolymer of an alkali activated precursor that has formed unstable gels such as sodium aluminosilicate hydrates and calcium aluminosilicate hydrates. This is possible through addition of a networking element, such as metakaolin, which will react with all excess cations [12].

2.4 Precursors

There exist several precursors for the making of geopolymers whereas many are waste or by-products from different industries. The major differences in the precursors lie in the composition of their constituting oxides. For geopolymers the most interesting elements are silica and alumina to form a silica-aluminate network.

2.4.1 Glass wool (GW)

In this project, glass wool (GW) waste is used as a precursor for making geopolymers. There are many types of mineral wool with glass wool and stone wool being the two most commonly used for geopolymers.

The most common application for GW is in insulating materials. GW consists of sand, limestone, glass fibers and multiple minerals which are glued together into a wool-like texture utilizing a binder, and thus the product ends up with a complex structure [14]. The final glass wool therefore consists of a mix of oxides. GW as insulating material may have varying composition depending on the application, and GW waste may have a larger variation as the waste is composed of GW made for different purposes. Comparison of the composition between different glass wool waste (15 samples from different geographical regions in Europe, and 18 samples from literature) have been made, and the median of each oxide is presented in Table 2.2 [1].

Table 2.2. Median composition of glass wool

Oxide	**Article [%]**	**Literature[%]**
CaO	8.19	7.41
SiO_2	62.70	63.60
Al_2O_3	1.86	3.50
Fe_2O_3	0.48	0.21
Na_2O	16.93	0.10
K_2O	0.56	15.34
MgO	2.48	1.23
P_2O_5	0.14	3.00
TiO_2	0.07	0.00
SO_3	0.41	0.06
MnO	0.31	0.17
Cr_2O_3	0.05	4.90
ZrO_2	0.01	0.01
SrO	0.02	0.00
BaO	0.00	0.01
NiO	0.02	0.08
CuO	0.01	0.00
ZnO	0.01	
PbO	0.01	
Cl	0.09	
Bi_2O_3	0.00	
LOI 525^oC	7.95	

The slight deviation between the median in the study and the literature is attributed to the geographical location of the collected waste.

The GW used in this project comes mainly from Saint-Gobain themselves. The waste contains mainly glass wool waste but also dried water-based acrylic pain, phenolic binder and water based adhesive.

The waste products are grounded to powder using a large ball mill. The powder is further sieved and the powder in the range <500 µm is used for making the cementitious materials.

Binder is added as one of the final steps during the manufacture of mineral wool to decrease the dusting and ensure that the product keep its shape after packing. The binder is an organic resin, usually phenol formaldehyde and the presence of organic compounds may affect the geopolymerization. The organic content can be determined by TGA as multiple components may vaporize when supplied to enough heat. An existing problem related to the organic binder is the ammonia emission, which increases with alkalinity.

$$NH_2CONH_2 + 2NaOH \leftrightarrow Na_2CO_3 + 2NH_3$$

The reaction is a result of the alkaline environment, and can be altered by changing curing conditions i.e., humidity and temperature. Further, it has also been stated that the organic resin may also results in emission of volatile organic compounds (VOC) [1].

It has been stated that the presence of an organic resin, can reduce the milling efficiency and increase the liquid demand. The development of the compressive strength in room temperature is also mitigated [16].

2.4.1.1 Properties of geopolymer from glass wool waste

GW as a precursor for alkali activated materials and geopolymers has in later years been of interest due to the potential replacement of OPC as binder in construction materials. A study was made with the aim of analyzing geopolymers based on glass wool from Saint-Gobain Isover with the pulverized particle distribution ranging from 1.3-24.4 μm in diameter. Sodium aluminate mixed with sodium hydroxide and water, with a 36,5 wt% concentration of the alkali was used. The study presented differences in properties between samples containing glass wool, with and in the absence of organic resin. Further, different curing conditions were used. Three samples with GW as precursor were prepared: GW1, GW2 and GW3. GW1 contained resin and was cured for 28 days in 22 °C. GW2 with resin, was cured 4 days in 50 °C and 24 days in 22 °C. GW3 contained no resin and was cured under the same conditions as GW2. The compressive strength is presented in Figure 2.11.

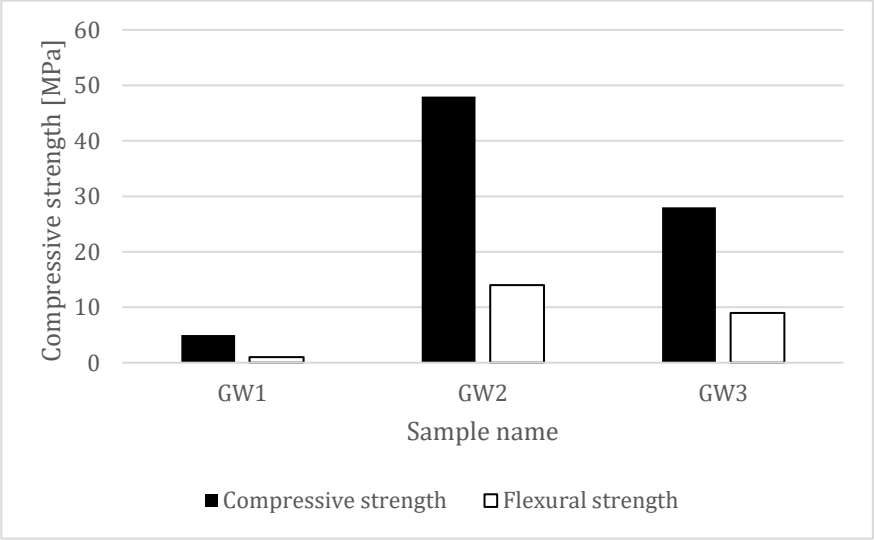

Figure 2.11. Data of GW1, GW2, GW3 from "Utilization of Mineral Wools as Alkali-Activated Material Precursor"[15]

Comparing GW1 and GW2, which differ in curing condition, it can be observed that not only the chemical composition has a significant impact, but also the processing parameters. The presence of organic resin also has an effect on the strength [15].

2.4.2 Metakaolin

Metakaolin is formed through calcination of kaolin clay. It is a controlled thermal treatment with the aim of obtaining high pozzolanic index. Due to its ability to obtain high pozzolanic properties, it's suitable to replace cement in concrete. Pozzolanic property is the ability of the silica and/or alumina in the material to react with calcium at ordinary temperature and in the presence of moist to form a cement which hardens [16, 17]. Metakaolin is an attractive precursor for cementitious materials but also as a networking element in the manufacturing of geopolymers [12]. The composition of metakaolin can vary, and the average composition is presented in Table 2.3 [18].

Table 2.3. Chemical composition of metakaolin [18]

Chemical composition	**Metakaolin [wt%]**
Silica (SiO_2)	50-60
Alumina (Al_2O_3)	30-40
Magnesium oxide (MgO)	0-2
Potassium oxide (K_2O)	0.5-1.5
Sulfuric anhydride (SO_4)	1-3
Calcium oxide (CaO)	0-0.5
Ferric oxide calcium oxide (Fe_2O_3)	0.5-5

The choice of calcination method will affect the properties of the formed metakaolin due to the formation of different aluminum-coordination of varying amounts. Presented in Table 2.4 are different common calcination methods and the percentage of different Al-coordination [12].

Table 2.4. Calcination method and Al-coordination content [12]

Calcination method	**Al-O-Al Al(IV)**	**Al=O Al(V)**	**Al-OH Al(VI)**
Rotary	15	50	35
Flash	20	55	25
Vertical	27	49	24

Al(V) is the most reactive and results in faster reaction and thus faster hardening. It is therefore of interest to have a high content of it [12].

2.4.3 Other precursors and additives

Commonly used precursors for alkali activated materials and geopolymers are slags from industries. Fly ash (FS) and ground granulated furnace blast (GGBS) are the two most commonly researched on. Fly ash is a fine powder residual from combustion of coal [19]. Ground granulated furnace blast is a by-product from iron in blast-furnace [20].

There are several reasons as to why additives can be attractive to include in the mixture. The advantages ranges from circular economy, less environmental impact and enhanced properties of the product. This project includes two types of slags as additives: Slag1 and Slag2. Slag1 has previously been presented as a good precursor in geopolymers and alkali activated materials leading to good mechanical properties. Slag2 has been presented to be suitable as asphalt additive, friction media or in soil stabilization [20].

2.4.3.1 Properties of geopolymer based on slag

Slag1 and Slag2 are from the steel industry and share many similar elements whereas Slag1 has a higher Si, Ca, Mg and Al content in comparison to Slag2. The composition of the different precursors and additives are presented under section *3.1. Materials*.

A research group have studied the microstructure and mechanical properties of fly ash/GGBS-based geopolymers with sodium hydroxide and sodium silicate as alkaline medium and with the samples cured at 70 °C for 24 hrs before additional curing in room temperature. The study included 0-60% GGBS. An increase in GGBS content resulted in a higher compressive strength. However, 30% and 60% content showed a negative trend between the 7 days and 28 days compressive strength measurements whereas the rest had a positive increase from 7 to 28 days [21]. Others have done a similar study however with

only curing in room temperature. Similarly, an increase in compressive strength was observed upon higher percentage of GGBS [22].

2.4.4 Ratios

There are certain ratios that are essential for geopolymerization as it will result in different networks being more favored to be formed.

2.4.4.1 Silica to alumina - Si/Al

Geopolymers are built on a foundation of aluminate-silicate network and thus the ratio between Si and Al is significant for the properties, and dependent on the precursor there are different optimum ratios. For metakaolin-based geopolymers the molar ratio of 1.65≥ results in a homogeneous binder with unreacted particles, and a ratio around 1.90 results in a decrease in porosity. The trend observed for metakaolin-based GPs is a decrease in compressive strength above molar ratio of 1.90 and has thus created confusions as the Si-O-Si bond is stronger than the Si-O-Al bond. The phenomenon has been explained by that the amount of unreacted particles is increased upon higher ratio and these act as point defects [23]. Other research results have proven the opposite. An increased ratio has resulted in higher strength and the authors believe that the unreacted particles act as solid state precipitation hardening [24].

2.4.4.2 *Water-to- alkali – H_2O/M_2O*

A high-water content in relation to alkali-silicate can result in migration of the cations from the reaction site and formation of unwanted by-products such as carbonates. Geopolymers are sensitive to ratios between different elements as an excess of certain elements can lead to migration and formation of unwanted side-reactions. The effect of alkaline activator ratio on the compressive strength of geopolymers based on fly ash has been investigated. It was done by analyzing different water glass/NaOH ratios which also results in different H_2O/Na_2O ratios. The latter ratio ranges from 9-12 where a maximum strength has been observed for H_2O/N_2O=11 before decreasing again [25].

There have also been studies on geopolymers based on fly ash with low calcium content and H_2O/Na_2O in the range 3-6.5, where decreasing compressive strengths have been observed for higher ratios [26].

2.5 Alkali reagents

There exist several types of alkali-reagents for geopolymerization. The most used is sodium hydroxide and alkali-silicates. The function of alkaline medium is to dissolve the precursor. The metal-cations in the solution will balance the negatively charged tetrahedral aluminum centers and thus enable the formation of oligomers. An excess of alkali cations will result in efflorescence through the migration of the cations to the surface. The reaction between the cations and carbon dioxide will result in the formation of alkali-carbonate [27].

2.5.1 Sodium hydroxide (NaOH) and potassium hydroxide (KOH)

Sodium hydroxide is regularly used as a reagent in geopolymerization. Apart from being cost effective, the solution has low viscosity and is easily manufactured. Furthermore, the alkali cation (Na^+) is small and is easy to transport in the network [28]. Higher concentration of NaOH results in well-dissolved precursor which empowers a good reaction. At high concentrations, NaOH lead to a highly acidic environment which compose a health risk for workers. Additionally, the acidity will damage the equipment [29]. A combination of NaOH and additional alkali-silicate is also being used. For this

approach, there is a need for dissolving the alkali-silicate in NaOH 24 hrs prior to mixing with precursor in order for the silicate to be fully dissolved and well distributed in the total solution.

In contrary to sodium, potassium ions are larger in size and thus there exist hindrance in transportation, which also explains the greater dissolution ability of NaOH. However, an increase in alkalinity of NaOH results in greater dissolution of Si to a certain upper limit, while KOH shows a proportionality beyond that of NaOH [30].

2.5.2 Alkali-silicates (K, Na-Si_xO_y) – Water glass

Alkali silicate solutions are also known as water glass. The alkali silicate, containing either sodium (Na) or potassium (K), is mixed with water. Sodium silicates are the most commercially used amongst the two, partly due to its economic benefit and partly due to the small size of the alkali ion. Alkali-silicates are available in different grades (different molar ratios of SiO_2/M_2O) and phases. This project deals with the liquid phase. Different ratios lead to different solubility and sensitivity to external environments. Higher molar ratios have lower solubility and are less sensitive to temperature, i.e., higher temperature is required in order to increase the solubility slightly. Sodium silicates can contribute to high mechanical strength under suitable curing conditions and composition, i.e., they are sensitive to the amount of different reactants [31]. Potassium silicates are similar to sodium silicates but less sensitive to changes. Potassium silicate also have a higher price.

Alkali silicates in AAMs and GPs have proven to result in good strength. Today, soluble silicates are amongst the synthetic chemicals that have the largest production volume. The negative environmental impact of water glass has however become an issue, and many have looked into the possibilities of recycling it or produce environmentally friendly alternatives. Silicon in the water glass becomes biologically active orthosilicic acid and thus affect the aquatic environment upon reaching the ocean [32]. Synthetic manufacturing routes include a melting process or hydrothermal process. In the melting process silica sand and sodium carbonate are let to react in a furnace under 1400^{o}C. The process requires high energy consumption and emits carbon dioxide, nitrogen oxide or sulfur oxide, and the equipment subjected to the chemicals are also attacked by the carbonates. In the hydrothermal process route silica sand and sodium hydroxide reacts in an autoclave under high pressures. The negative impact includes large water consumption, aggressive working conditions and high energy consumption required to reach high pressures [33].

2.6 Curing temperature and curing time

It exists a study on a wide range of curing temperatures for metakaolin-based geopolymers (30-90 ^{o}C) with the use of thermal analysis methods including DSC. The samples were cured for 24 hrs. The authors presented the conclusion of an optimum curing temperature of 60 °C. This temperature showed the highest heat release, which indicates a favorable polycondensation. Higher temperatures result in fast kinetic and lead to the formation of a large number of Si^{4+} and Al^{3+} species, which form a gel-coating on the metakaolin and prevents it from further dissolution and thus preventing further reaction. Lower temperatures lead to low reaction kinetic which result in a low dissolution of metakaolin. There are also entrapped water in the pores which hinders gel-formation and thus resulting in a higher degree of porosity [34].

Another investigation further confirmed the results. However, this study investigated temperatures 20-100 ^{o}C cured for 1 h, with the highest strength achieved at 60 ^{o}C after 7 days of curing. Their arguments as to why the higher and lower temperatures resulted in lower strength were the same [35].

A relation between curing time, pH and compressive strength has also been presented [31]. An increase in mechanical strength can be observed as Al-coordination transforms from Al(V) to Al(IV). Pending

strength with a slow increase occur as Al(IV) forms Al(VI) which is the final Al-phase. Further curing results in depolymerization. As the polymerization restarts, an increase in strength reoccurs. Lower pH has also been seen to promote higher strength.

2.7 Phases in geopolymers and AAM

2.7.1 N-A-S-H (Sodium aluminosilicate hydrate) and K-A-S-H (Potassium aluminosilicate hydrate)

(N, K)-A-S-H gel is the main product in AAMs with either Na^+ or K^+ as the metal cation as charge neutralizer of the negatively charged alumina centers (AlO_4^-), whereas N-A-S-H is more commonly found due to higher content of sodium in many precursors and in many alkali-solution. The following section will thus refer to N-A-S-H. The gel-structure seen in Figure 2.12 (right) contribute to a structural instability due to the presence of cations along the edges of the structure. This in combination of the presence of water results in transportation of cations from the areas in which reaction take place, and thus no stabilization of the negatively charged alumina centers. Figure 2.12 presents a reaction resulting in the formation of a M-A-S-H where M is either K or Na [36].

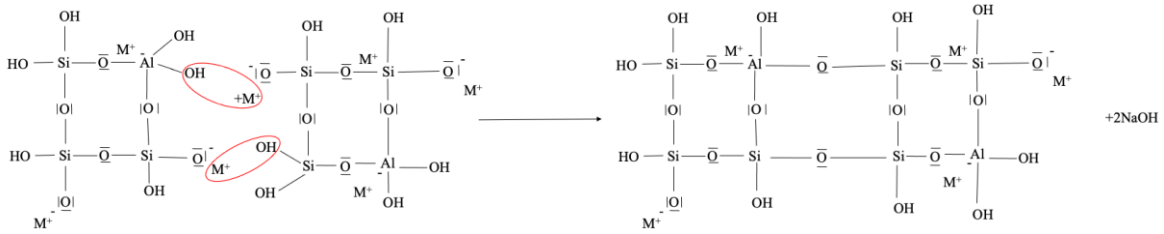

Figure 2.12. Formation of (N, K)-A-S-H

The gel is a tetrahedral network with alternating silicon and aluminum connected to oxygen and Al-centers stabilized with M^+, as presented in the figure above. Analysis with NMR has shown that the silicon is predominantly $Q^4(3Al)$ and $Q^4(2Al)$ units where Q^4 describes the environment of the central silicon, i.e., silicon being connected to 4 silicon-species. N-A-S-H is by ordinary found in systems with low calcium-content [36].

Type of alkali-solution, reaction kinetics and curing temperature have demonstrated to affect the nature of the gel. Silica and sodium content, and molar ratio (grade) of the alkali-solution affects the degree of polymerization and thus the formation of intermediate products, i.e., gels. Si/Al ratio in the system does not affect the N-A-S-H structure significantly. Further, the presence of high amounts of N-A-S-H can influence the kinetics of other reactions [36].

N-A-S-H and other gels are of amorphous nature, which can be observed in analysis including TGA and XRD.

N-A-S-H is commonly found in AAM and does not exist in stoichiometric geopolymers, which are geopolymers containing right amounts of reactants that will fully react with each other and thus leaving no excess that can precipitate or participate in other reactions that may potentially be harmful for the strength of the formed cementitious material. Figure 2.13 show the difference in composition between N-A-S-H and stoichiometric geopolymers [37, 38]. Difference between geopolymers and AAM is presented under section 2.3.2 *Geopolymers vs alkali activated materials.*

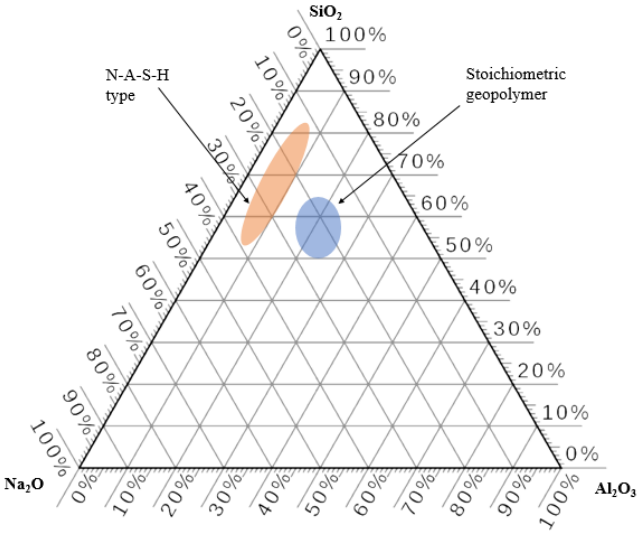

Figure 2.13. Ternary diagram showing N-A-S-H and stoichiometric geopolymer

2.7.2 C-S-H (calcium silicate hydrates) and C-A-S-H (Calcium aluminosilicate hydrate) and C-(N)-A-S-H

C-S-H phases are commonly described as gels due to the absence of long-range order. C-S-H phases are characterized by a high calcium content and with stoichiometric variation in the composition [39].

C-S-H has a structural resemblance to tobermorite structure with a maximum Ca/Si ratio of 1.40 but more commonly ranges between 0.67-0.83. It consists of nanocrystalline clintobermorite, amorphous calcium hydroxide layer and gel pore water. It has sheets consisting of calcium and oxygen, which are surrounded by tetrahedral silica in a tetrahedral structure. The interlayer between the sheets is mainly occupied by water. During the reaction, calcium hydroxide ($Ca(OH)_2$) is formed which can further participate in pozzolanic reactions with supplemental cementitious materials to form C-A-S-H under the right conditions [40, 41]. C-A-S-H is a reaction product found in alkaline cement with high calcium content. The compositional region in which C-A-S-H has been found vary slightly, and there is a region in which both N-A-S-H and C-A-S-H can be found denoted C-(N)-A-S-H. Ternary diagram presented in Figure 2.14 presents regions in which the two gels have been observed [38, 42-44].

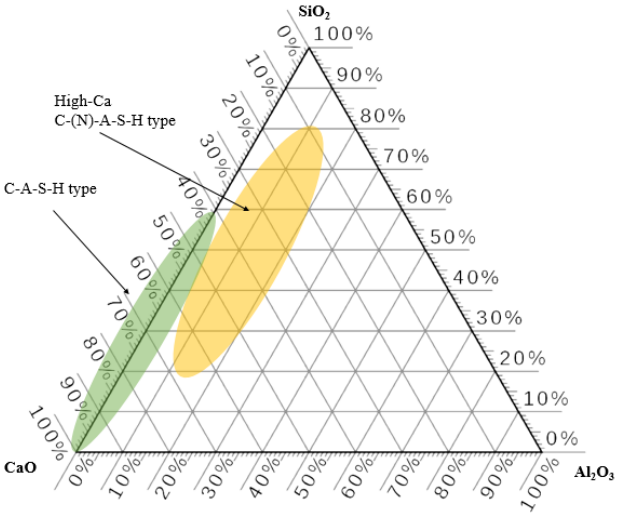

Figure 2.14. Ternary diagram showing C-A-S-H and C-(N)-A-S-H

Similar to C-S-H, C-A-S-H has silicate in a tetrahedral structure which are connected through a dreierkette structure. Equivalently to N-A-S-H, the type and ratios between elements in the alkali-solution and in the system determines the nature of the formed gel. NaOH and water glass have been presented to induce differences in the structure. NaOH as the alkaline source lead to aluminum in $Q^2(1Al)$ in bridging positions and low Q^3 content whereas water glass presented a higher percentage of aluminum with high Q^3 content. The higher Q^3 is an indication of intertwining between chains in the structure, and some lamellae structure in other areas [45].

2.7.3 Other phases

GPs and AAMs are highly sensitive to ratios between certain elements. Higher or lower content of certain species enables formation of certain phases. Some minerals are commonly found in these materials due to their natural existence in the raw materials. This includes quartz, which is a constituent in metakaolin. Minerals are crystalline materials and thus can be identified with XRD.

Quartz has the chemical formula SiO_2 and belongs to the trigonal crystal system. It's one of the most commonly found minerals [46]. It's strongest XRD peaks are found around 2Θ = 20.9°, 26.6°and 50.0° [47].

Gaylussite has the chemical formula $Na_2Ca(CO_3)_2{\cdot}5H_2O$ with monoclinic crystal system and a brittle nature [48]. Its strongest XRD peaks can be found between 15-60° with strong peaks around 18°and 30°[49].

Mullite, also known as porcelainite, has the chemical formula $Al_{4+2x}Si_{2-2x}O_{10-x}$ with x~0.4 and belongs to the crystal system orthorhombic. It can be formed from kaolinite and thus may be visible in samples containing metakaolin. Impurities may exist in the structure with titanium, iron, sodium and potassium being the most common [50]. The characteristic XRD peaks of mullite include the region 15-65° with the strongest peaks presented 15-30° and an area with slightly lower intensity between 30-45°[51].

Nepheline has the chemical formula $Na_3K(Al_4Si_4O_{16})$. It belongs to the hexagonal crystal system and has a brittle nature[52]. The characteristic XRD peaks can be found between 15-40° with the strongest being visible between 20-30°[53].

Calcite has the chemical formula $CaCO_3$ and it belongs to the trigonal crystal system and has a brittle nature. It can be found in various forms and colors and has high reactivity in the presence of acid [54]. The characteristic XRD peaks of calcite include 20-45° with the 29.2° being the strongest peak [55].

2.8 Characterization

2.8.1 Calorimetry

Calorimetry is measurement of the heat release or absorption during a chemical reaction, and thus showcasing if the reaction is exothermic or endothermic. Calorimetry is commonly associated with a direct way of receiving data of thermal properties, and often at higher temperatures. There are multiple ways of obtaining such information and DSC (Differential scanning calorimetry) is often used in the research field. It is an effective tool which can give information related to characteristic melting temperature, crystallization and mesomorphic transitions. Further, enthalpy and entropy changes can be extracted which further provides information of the glass transition. Advantages of this technique includes a broad dynamic range in the heating and cooling process [56]. The technique is based on comparison between two chambers: one empty which operates as reference, and a chamber containing the sample.

However, there are alternatives to DSC which can provide simple estimations of the heat- and cooling, i.e. reactivity if there are exothermic or endothermic reactions occurring, phenomenon of a sample. A simple set-up is in the form of two thermometers and a temperature/data logger. A sample and a reference sample can each be connected to a thermometer and changes in temperature can be monitored through the logger. A difference in temperature between the sample and reference indicates a reaction taking place, and by applying Equation 1

$$Q = mCpdT \tag{1}$$

with known temperature difference between reference and sample (*dT*), specific heat capacity (*Cp*) and the mass of the sample (m), the total heat loss or gain (*Q*) can be calculated.

2.8.2 Mechanical measurement

Tensile instruments can be used to measure stress as a function of strain. The obtained curve describes the nature of the material as it is subjected to a force. Presented in Figure 2.15 is an example of a stress-strain curve. The first region is called *Elastic region* as the material behaves elastically, i.e., it can return to its original shape after the force has been removed. The end of the elastic region and start of the plastic region is called *Yield point* and stretches to the *Fracture point* at which the material breaks. Cementitious materials are by nature brittle and thus contains no or very small plastic region. The maximum strength is called ultimate tensile strength (UTS) [57].

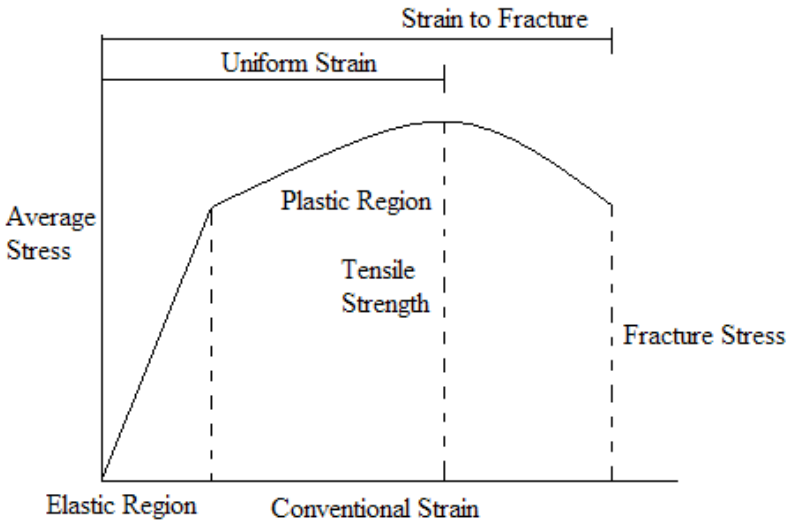

Figure 2.15. Stress-strain curve showing different characteristic regions in which a material can have. [58]

For compressive strength measurements the sample is put between a stationary and a movable metal head which applies force onto the sample, as seen in Figure 2.16. On a monitor connected to the tensile instrument, stress is registered as a function of strain.

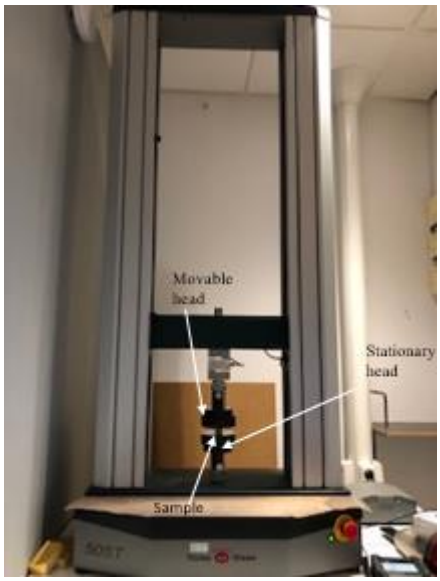

Figure 2.16. Tensile machine for compressive strength measurements

2.8.3 X-ray diffraction (XRD)

XRD (X-ray diffraction) is a technique that provides detailed information about crystallographic structure, phases, texture, grain-size along with physical properties of the crystalline materials [48]. There exist two types of XRD-techniques: single-crystal XRD and powder XRD, where the major difference lies in sample preparation. X-rays are emitted towards a sample target, from an X-ray source, and a collimator enables a thin X-ray beam with a narrow spread of wavelengths. When the X-rays hit the sample a diffracted pattern characteristic of the crystal structure is obtained. The phenomenon originates from Bragg's law. The uniform spacing between atoms in the material causes an interference pattern from the incoming X-rays, see Figure 2.17.

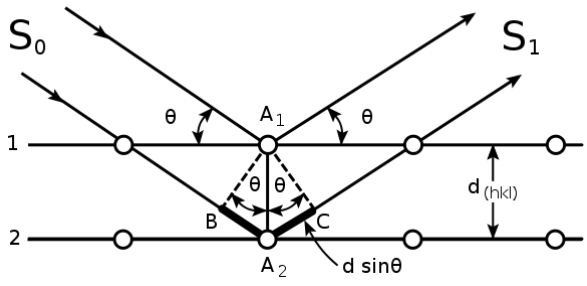

Figure 2.17. Diffraction in crystal planes based on Bragg's law [59]

The pattern is presented as intensity against the angle of the detector, and provides information to determine the crystal planes of the structure and giving the lattice and thus the unit cell. Materials acquire unique diffraction pattern and XRD, see instrument in Figure 2.17, is thus an efficient tool to determine the constituting elements [60].

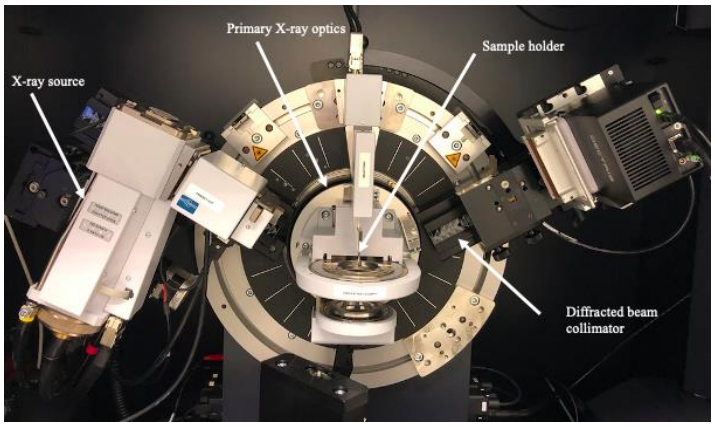

Figure 2.18. XRD instrument with some main components marked

XRD is essentially used for analysis of the periodicity of the material lattice which is expressed by distinct sharp peaks. Amorphous materials give broader peaks due to a lack of periodicity and are therefore harder to distinguish. However, the broader peaks give an indication of the phases (material crystal structure) and the pattern can thus provide complimentary information to results obtained from other analysis methods. Databases and/or articles providing characteristic peaks for crystals can be used to compare and thus find phases present in a sample. Characteristic peaks for multiple minerals found in AAM and geopolymers can be found under section 2.7.3 *Other phases.*

2.8.4 Thermogravimetric analysis (TGA)

TGA (Thermogravimetric analysis) analyses the thermal stability of a material and presence of volatile components by observing the change in sample weight as the heat is increased at constant rate. This is done in the presence of an inert gaseous atmosphere which removes potential gaseous by-products. This allows the sample weight to be correctly monitored in a furnace located at the center of the instrument, see TGA instrument in Figure 2.19.

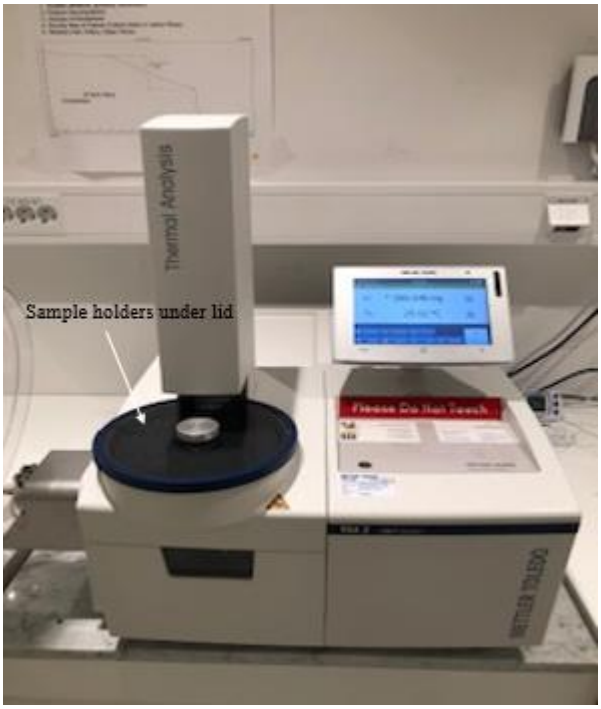

Figure 2.19. Thermogravimetric analysis instrument

There exist three types of TGA: dynamic, static and quasistatic. Dynamic TGA has a continuous uniform increase in temperature over a set period of time, and the mass is recorded as a function of the temperature. This method can provide the mass of the gas that is removed. Static TGA is a method where the sample weight is monitored as the temperature is constant. This method allows information of how well a material can withstand a temperature of interest. Quasistatic TGA is a method in which the sample is heated at different temperatures. A graph presenting sample weight/weight loss as a function of time or temperature can be obtained [61]. Volatile compounds are disposed from the sample followed by less volatile ones. Species have characteristic decomposition temperatures or time at a set temperature, and thus allowing identification of the content. DTG is the derivative of the curve which proves the weight loss against temperature/time. From the derivative, phases can easier be identified as changes are presented more distinctively.

TGA for GPs and AAMs have characteristic weight drops. The weight drops at 0-120 °C are due to evaporation of the physically bound water, i.e., water in pores, surface and between layers of other phases. Weight loss between 120-200 °C are commonly related to evaporation of chemically bound water including those in gels such as N-A-S-H and C-A-S-H. There is no distinction between the type of gel-structure due to many chemically similar characteristics. Double peak between 100-200 °C has shown to indicate the presence of calcium alumino hydrates with zeolite water [62].

Between temperatures 300-800 °C it is believed that the continuous weight loss attributes to the melting and decomposition of the phenolic resin in GW [43]. This region is also ascribed to destruction of structural water from condensation of silanol and alumino groups from gel-structures [63].

The region of 700-800 °C, may have multiple origins. Melting of organic resin, and thus release of all water that has been entrapped in possible pores, has been observed in this area in previous studies. Samples containing carbonate may also have a peak in this region. Possible carbonate compounds in AAMs and GPs include calcite for samples with higher calcium content and sodium carbonate for those containing higher sodium content [43]. The source of carbon includes the phenolic binder but also cations in a reaction with carbon dioxide in the atmosphere resulting in the formation of carbonates [64].

2.8.5 Optical microscopy

Optical microscopy is a technique using visible light and a combination of lenses to magnify surfaces. It is the oldest and simplest type of microscopy. However, with additional components to improve resolution the instrument can become more complex. The resolution reaches approximately 200 nm and a magnification of 1000x [65].

Microscopes today are connected to a software which enables capture of digital images of the magnified samples. Eyepieces are commonly a part of the microscopy but with software, images can be displayed directly on the computer.

More advanced alternatives to light optical microscopy includes scanning electron microscopy (SEM) and transmission electron microscopy (TEM) which can be connected to an additional instrument for identification of elemental compositions [66]. Figure 2.20 shows a classical optical microscopy.

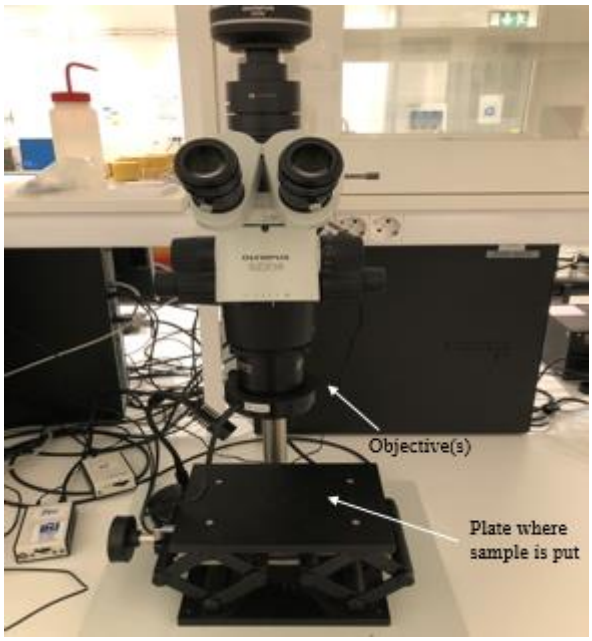

Figure 2.20. Optical microscope

3 Experimental method

The experimental part is essentially comprised of three steps: determination of reactivity, making of wet geopolymer paste and characterization.

3.1 Materials

The method for mixing is highly related to the amount and type of the different components. Use of additives will also affect the required mixing time. The investigated components were the following: Glass wool powder (ball milled into a size of <500 µm) from Saint-Gobain, metakaolin, water glass (mixed sodium and potassium with higher content of sodium, total solid content being 41.7 %), Slag1 and Slag2. The average composition of the dry raw materials is presented in Table 3.1, with the composition of slag representing both types. They are similar in composition with Slag1 having a higher Si, Ca, Mg and Al content in comparison to Slag2.

Table 3.1. Weight percentage of oxides in the components/raw materials

Component	**SiO_2**	**Na_2O**	**CaO**	**MgO**	**Al_2O_3**	**K_2O**	**Fe_2O_3**	**TiO_2**	**SO_3**	**H_2O**
GW [1]	62.7	16.93	8.19	2.48	1.86	0.56	0.48	0.07	0.41	
MK [18]	30-40		0-0.5	0-2	30-40		0.5-5		1-3	
Slag [67]	33.45		41.70	5.99	13.46	0.29	0.31	0.84	2.74	

Figure 3.1. GW, MK, Slag2, Slag1, water glass (raw material)

3.2 Laboratory work

The laboratory work comprised an initial reactivity test to determine the reactivity of the constituting components followed by making of the wet paste.

3.2.1 Reactivity

Reactivity of the components were analyzed to determine mixing order in the making of the geopolymer paste. The amount of dry component was predetermined followed by addition of alkali solution until a workable paste was achieved and similar viscosity was obtained for all samples.

Analysis was performed using a simple calorimetry set-up to compare the rise in temperature of each component in relation to one another. The reactivity order was used to determine the mixing order of the components with the order being from least to most reactive.

3.2.2 Wet slurry

17 mix designs were prepared, see Table 3.2. It's desired for the dry content to have a high content of glass wool waste. Potential additives including metakaolin and slag have shown promising results in this field and thus are of interest to incorporate into the mix composition to increase the mechanical properties. MK S was set to be the standard mixture for investigating curing time and temperature, and for comparing the effect of Slag1 and Slag2. The composition with 60% GW and 40% MK was based on previous studies done at Ecophon. The amount of water glass was also based on previously done studies with minor modifications. No extra water was added for mix compositions used to examine curing time, temperature and effect of slag. This was to eliminate the effect of water.

L/S stands for liquid-to-solid ratio with liquid being the sum of water glass and water. w/b is water-to-binder ratio with the water being the sum of the extra added water and the water in the water glass, and the binder being all dry components including the alkali-silicate in the water glass.

Table 3.2. Studied mix designs

Sample name	Glass wool (GW) [%]	Metakaolin (MK) [%]	Slag1 [%]	Slag2 [%]	Water glass (MR=1.7) [g]	Extra water [g]
MK S (standard)	60	40			290	
Slag2 S	60	20		20	290	
Slag1 S	60	20	20		290	
100%GW S	100				365	
90%GW S	90	10			350	
80% GW S	80	20			320	
70%GW S	70	30			305	
20%Slag1 S	60	20	20		290	
20%Slag2 S	60	20		20	290	
0.8L/S A	60	40			210	40
0.8L/S B	60	40			180	70
0.8L/S C	60	40			165	100
0.8L/S D	60	40			145	120
1.0L/S A	60	40			290	
1.0L/S B	60	40			270	15
1.0L/S C	60	40			310	15
1.0L/S D	60	40			200	90

The general procedure for the making of the slurry was performed with a Kenwood mixer with the following steps: dry powder was mixed until a homogeneous powder mix was obtained, alkali-silicate was gradually added under stirring (and tap water is then added gradually added under stirring). When all components have been added, the slurry was further mixed.

The slurry was poured into a silicon casting mold containing nine 20x20x20 mm cubes. The paste was poured onto the mold under shaking which allowed the paste to sink into the holes evenly. The mold was then shaken with shaking table and sealed with a plastic bag (to avoid rapid evaporation of water), and put into the oven.

Figure 3.2. Experimental steps

After curing in oven, the samples were demolded and kept unsealed in room temperature with an average humidity and temperature of 30% and 15 °C respectively until compressive strength measurements were performed after 7 and 28 days of curing.

Studied time and temperature combinations are presented in Table 3.3.

Table 3.3. Studied curing temperature and time

Curing temperature [°C]	**Curing time [h]**
40	4, 6, 24
60	4, 6, 24
80	6, 24
RT	

Investigation of mix composition (GW content and addition of slag) was performed at 60 °C and 4 hrs.

3.3 Characterization

3.3.1 Calorimetry measurement

In this experiment, the paste was put in a sealed plastic container equipped with a sealed pipette that act as a holder for a temperature sensor attached to a temperature data logger (Testo Saveris 2). The changes were measured and presented as temperature vs time. The reference contained GW and water.

3.3.2 Mechanical measurements

The compressive strength was measured with a UMD testing machine after 7 days and 28 days of curing. The samples are of dimensions 20x20x20 mm. The rate of the head, towards the sample was 100 mm/min. The results are presented as strain vs position, which could further be translated into stress vs strain.

3.3.3 XRD

The sample with highest compressive strength was analyzed with XRD in order to identify phases that could explain the strength. Other samples were also analyzed in order to see potential differences in formed phases, between the samples.

The samples were put in isopropanol after 28 days of curing to stop further reactions. Prior to measurements, the samples were dried at 40 °C for 24 hrs before being milled into size < 75µm. Powder XRD measurements were performed at CMAL – Chalmers Materials Analysis Laboratory with copper K_α radiation source to investigate the phase composition of the specimen. Each sample was measured for 15 min.

3.3.4 TGA

Samples were investigated with TGA in order to identify phases that could explain the strength. Samples containing Slag1, Slag2 and 100%GW were also analyzed in order to see potential differences in formed phases.

Dynamic TGA was performed. Sample preparation consisted of crushing the cubes into fine powder and filling crucible with 25-35 mg of sample. The temperature program was set to an increase of 10 °C/min until 800 °C was reached.

4 Results and Discussions

In this section, results from reactivity test, XRD, TGA, compressive strength measurements and optical microscopy will be presented and discussed.

4.1 Calorimetry

The samples contain more than one component leading to unknown specific heat capacity of the formed material. A calorimetric curve with heat release as a function of time was not of interest. The simple calorimetric set-up was performed only to see if a reaction was occurring.

Figure 4.1 presents the reactivity of used raw materials in order to determine the mixing order. The reference contains GW and water, i.e., no alkaline medium and thus no reaction. Slag2 has the highest reactivity followed by Slag1. GW and MK have similar reaction kinetic, and due to time-efficiency being of importance in the industry, the raw materials were approximated to be equal in reactivity for future mixes. Slag1 and Slag2 have a significantly faster hardening in room temperature, compared to MK and GW. Slag2 hardened to an unworkable paste within 6 minutes and Slag1 within 4 minutes and therefore leading to bad workability.

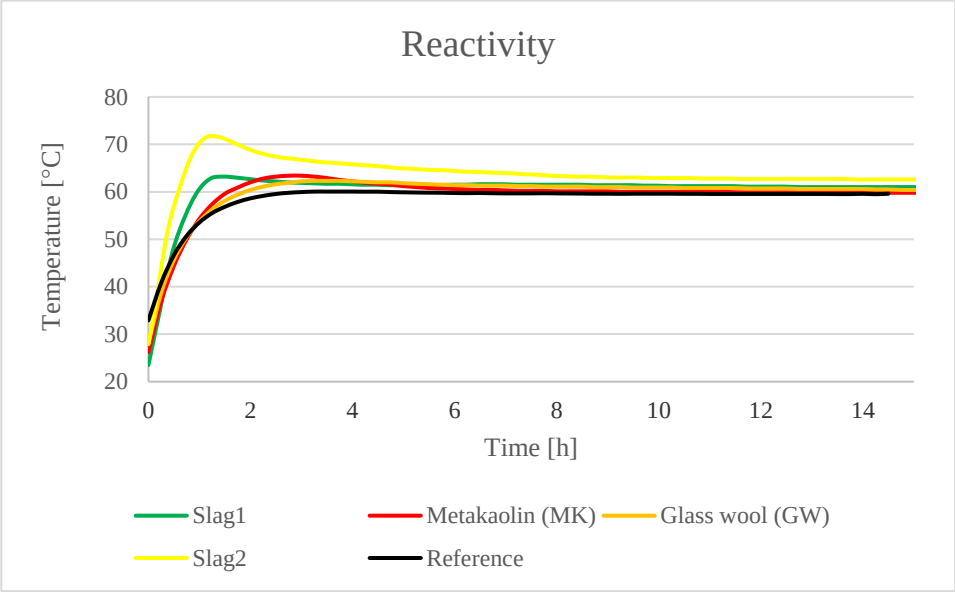

Figure 4.1. Reactivity of geopolymer components (raw material)

Letting raw material with different reactivity react with water glass simultaneously results in only the most reactive component being dissolved. GW was the main precursor but also showed the lowest reactivity and thus it was important to let it get in contact with the water glass in order for it to get sufficient time to dissolve.

4.2 XRD

Samples containing GW, MK, Slag1 and Slag2 were investigated in order to study the differences and similarities between the formed phases, and to see the possibilities in using Slag1, Slag2 and MK as addition in future applications. XRD spectrum are presented in Figure 4.2.

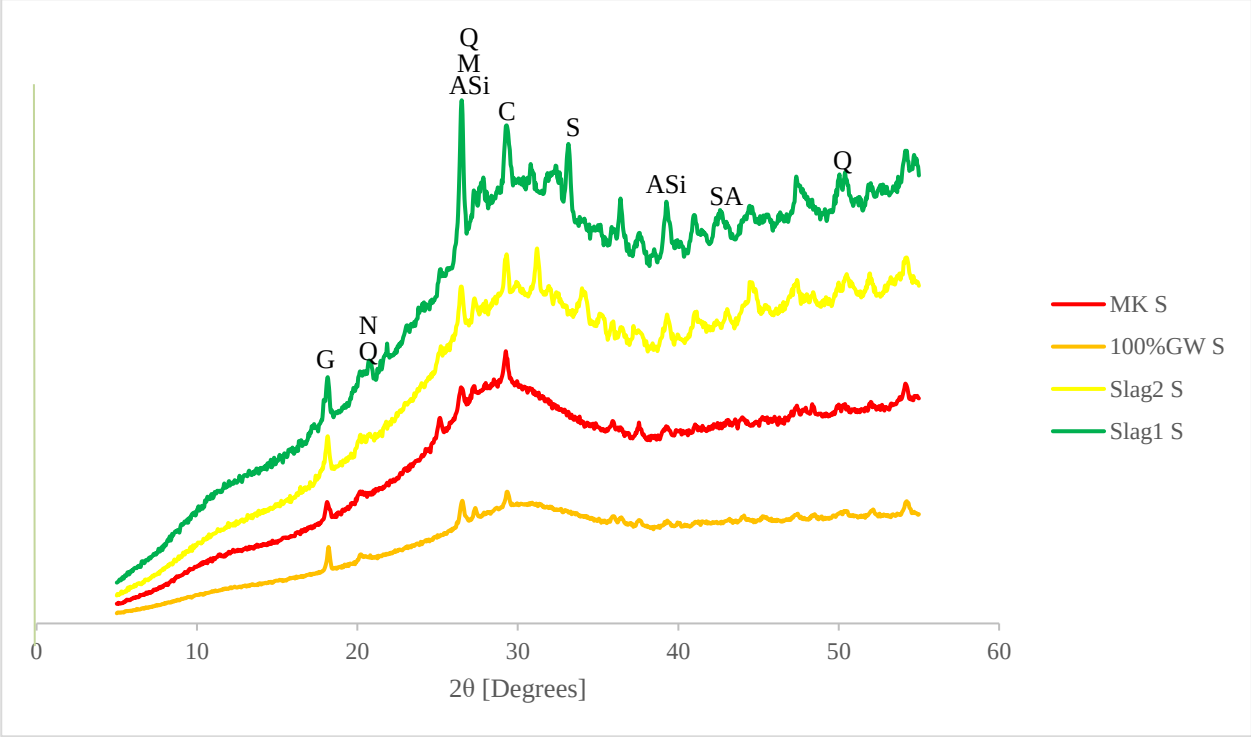

Figure 4.2. XRD spectra of MK S, 100% GW S, Slag2 S and Slag1 S. G-gaylussite, N-nepheline, Q-quartz, M-mullite, ASi-aluminosilicate, S-calcium sulphate, SA-sodium aluminate.

The rising shape between 20-40º is characteristic for amorphous materials and the intensity of the same peaks varies between the samples. Peak at 18.2º is a strong indication of gaylussite. The peak at 20.45 °C indicate the presence of nepheline. 100%GW S contains little Al and thus explains why it displays a lower intensity. For all samples except 100%GW, 20.45º also represents quartz which is present in metakaolin. Peak 26.45 °C is characteristic for the presence of aluminosilicate, and is in accordance to mullite. Peak 29.2º indicates a weak nepheline and strong calcite peak. The intensity at this angle is from high to low the following: MK, Slag1, Slag2 (with the two latter ones not differing much from each other). From the ternary diagram of CaO, Al_2O and SiO_2, see Figure 4.3, it can be observed that MK doesn't contain much C-(N)-A-S-H, leading to that the main reaction of the calcium goes to the formation of calcite and thereof showing a strong calcite peak. Slag1 and Slag2 both show lower intensity, likely due to that the calcium in the samples participate in the formation of both the gel structure and calcite. The region around 30º is also characteristic for the presence of a gel-structure, further proving the presence of N-A-S-H and C-(N)-A-S-H.

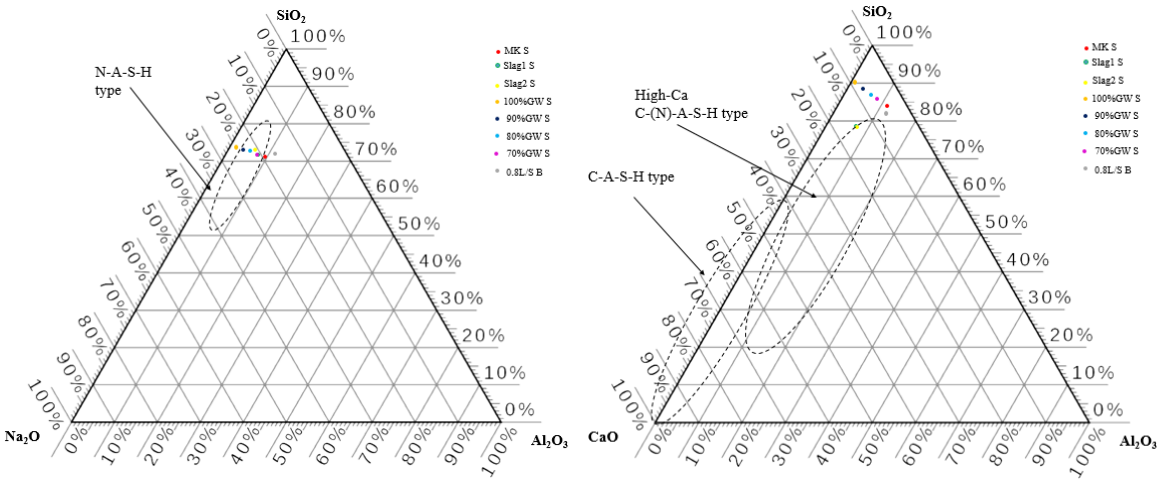

Figure 4.3. Ternary diagram of studied samples.

4.3 TGA

Figure 4.4 presents the DTG of all the samples, with TGA and DTG of individual raw material found in Appendix B. Many peaks are the same for all samples, showing that same or similar phases are present but differ in quantity. Region 0-100 °C is related to evaporation of the physically bound water. In the DTG, 100%GW S has the largest decline due to containing the highest amount of water amongst the samples. The other samples show a broader peak in the 100-200 °C region compared to the 100%GW S which attributes to the presence of a gel-structure. Seen in the ternary diagram, the majority of the samples have compositions in the region where N-A-S-H is favored to be formed. MK S is seen to be on the boarder and thus may contain less of the gel structure. 100%GW S, on the other hand, contains too low amount of Al in order to form N-A-S-H. Slag2 S displays a double peak in this region which is likely due to the presence of calcium alumino hydrates, i.e., C-(N)-A-S-H, with a lower calcium content.

Weight loss from 300-800 °C is related to the presence of organic resin as the TGA/DTG result of GW raw material show multiple phase transitions which align with the peaks in the samples, see Figure 4.4 and 4.5.

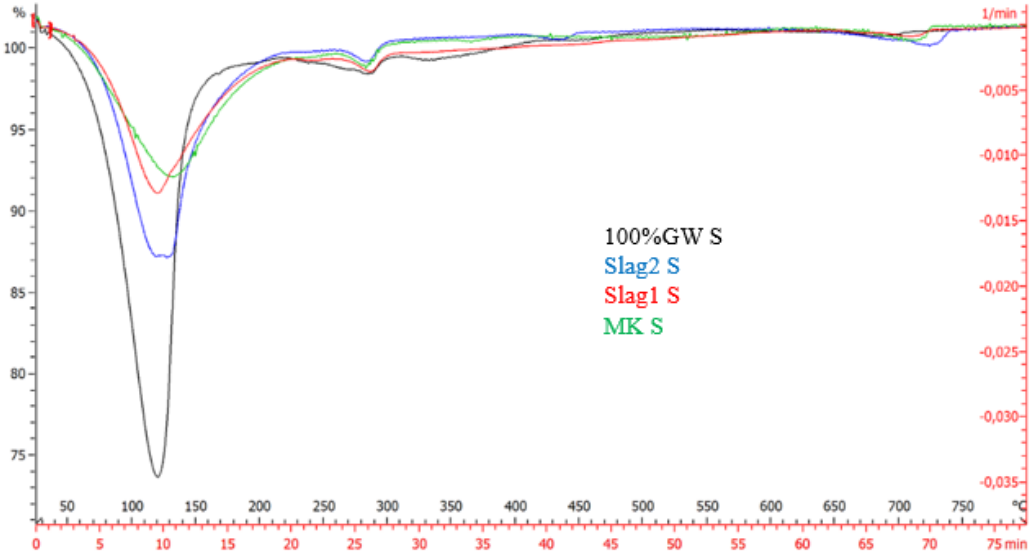

Figure 4.4. DTG of samples containing only GW, addition of MK, Slag2 and Slag1 respectively.

A decline equal to 1% between 1-100 °C for powdered GW raw material is attributed to the hardened water based PV/Ac adhesive in the GW waste.

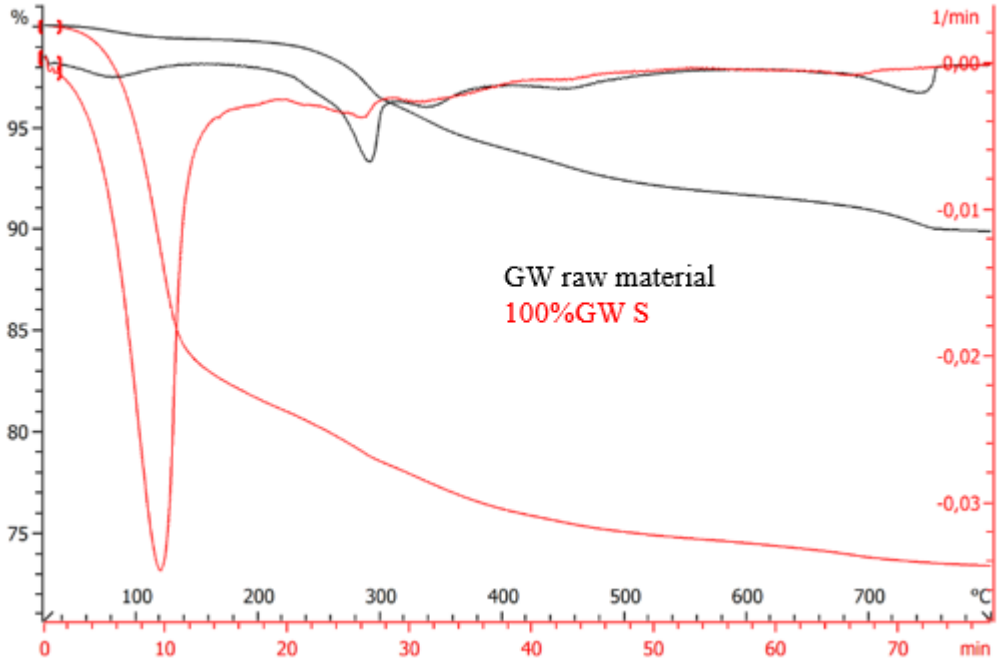

Figure 4.5. DTG and TGA of 100%GW S and GW raw material

Amongst the samples, 100%GW S has the largest peak at 300 ºC but has a smaller peak between 700-800 °C. Comparing the raw materials in all samples, see Figure 4.6 and 4.7, it can be observed that for all samples the peak at 300 °C is attributed to the GW raw material. Furthermore, given that region 300-800ºC show phase transitions related to the organic resin, it is believed that most components in the resin is decomposed at 300 °C and the rest decomposes/melts between 700-800°C. This would explain why the latter peak is smaller. Additionally, XRD measurements indicated the presence of calcite. For specimen including Slag2 and Slag1 the peak between 700-800 °C may therefore also represent the decomposition of carbonates. There are multiple sources to carbonate including the cations migrating to the surface and reacting with carbon dioxide. The phenolic groups in the GW binder is an additional carbon source. The XRD spectra show multiple calcite peaks whereas 29.2° is the strongest and thus supports the existence of calcite and calcium-based phases.

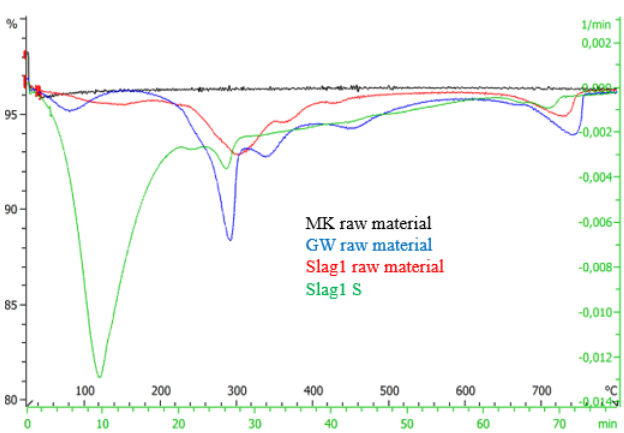

Figure 4.6. DTG of Slag1 S and its raw materials

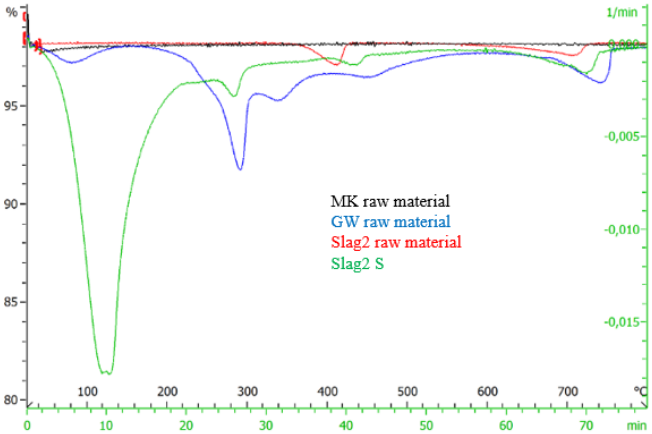

Figure 4.7. DTG of Slag2 S and its raw materials

4.4 Curing temperature and curing time

Results from analysis of curing time and temperature are presented in Figure 4.8. Samples cured at 40 °C, 6 hrs or longer could be demolded easily. Samples cured at 40 °C, 4 hrs was still moist and was left in room temperature in the mold for an additional 2 hrs before being demolded. All samples at this temperature displayed early strength development followed by a decline in strength between 7 and 28 days which is uncharacteristic for both AAMs and GPs. The difference in strength between the two measurements are statistically insignificant. However, a standard deviation up to 10% has been allowed which make the differences significant in further studies.

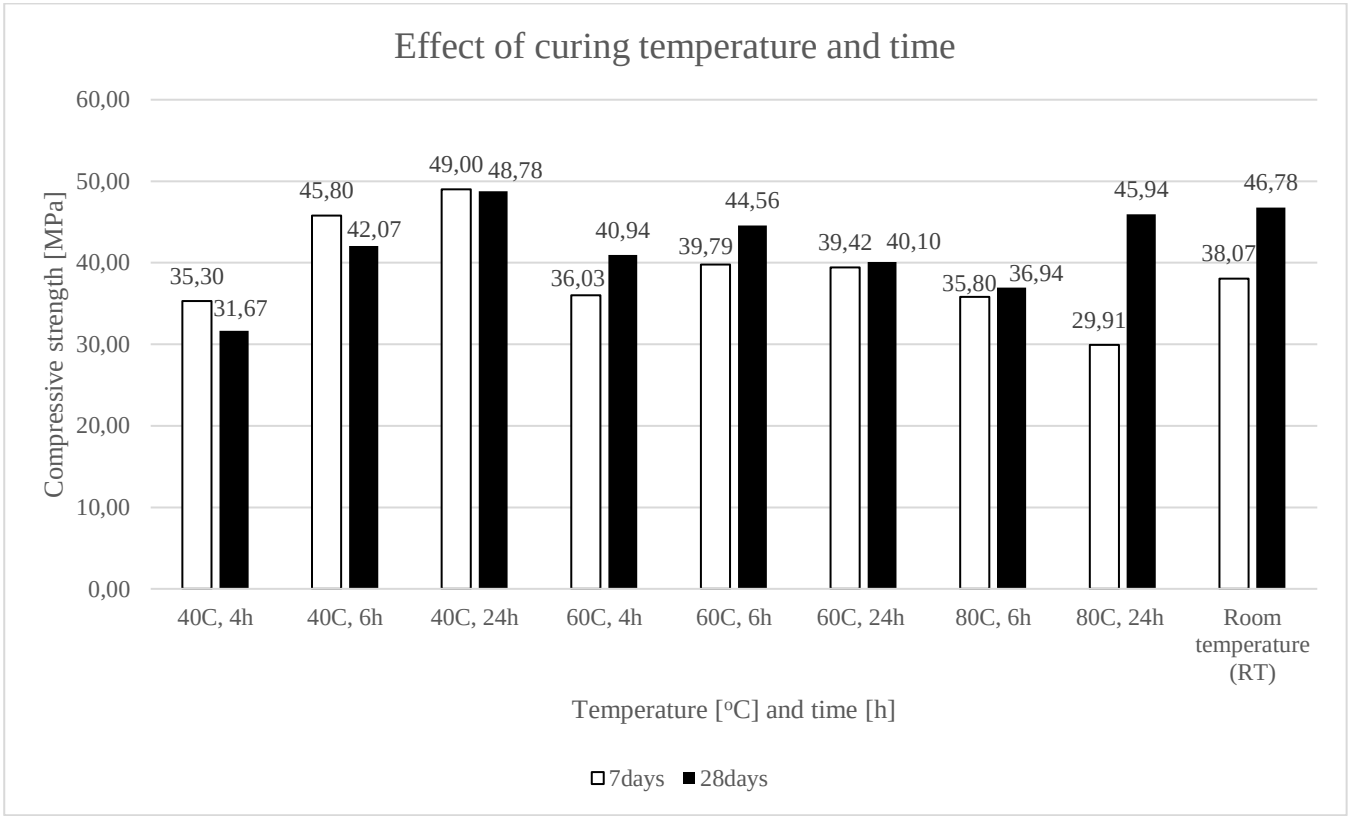

Figure 4.8. Effect of curing time and temperature on the compressive strength

Sample cured at RT was still moist after 24h and could be demolded after 48 hrs. The results support literature as lower curing temperatures in oven have been more favorable. However, 80 °C, 24 hrs contradicts by displaying a higher strength at longer curing time. RT curing showed no significant exothermal behavior, which is believed to be due to the much larger environment leading to the rate of exothermal reaction in the sample being equal to the rate of heat gain from the environment. Long RT-curing is believed to allow the silicates, aluminate and cations to react slowly and forming a stable structure. In comparison to literature, this study uses lower content of metakaolin and there is thus no need for dissolution of that raw material to the same extent. Further, higher curing temperatures allows for a shorter curing time. Observing the trend for 60 °C, it can be seen that the difference between 4 hrs and 24 hrs is not large indicating the possibility that after accomplished reaction, further curing can result in depolymerization of the structure.

4.5 Mechanical measurements

The curing temperature and time chosen for the investigation of slags and GW content was 60 °C and 4 hrs respectively as this combination showed to result in a good enough strength development, time efficiency and cost efficiency compared to previously applied curing time and temperature of 24 hrs and 60 °C at Ecophon.

The components (Slag1, GW, MK, Slag2) differ in the amount of liquid required to make the paste workable and thus can't contain the same L/S ratio unless water is added. However, water was not added due to the strength being negatively affected by increased w/b. The samples therefore contain different amounts of liquid, i.e., different amounts of water glass.

In Figure 4.9, the compressive strengths against the percentage of glass wool in the dry mix are presented. The trend is a decrease in strength upon higher GW-content. This is believed to be due to the decrease in Al (higher Si/Al ratio) which prevents the formation of the stable alternating Al and Si tetrahedral network. -Si-O-Si- bonds are chemically stronger due to a stronger covalent bond between the atoms. However, the opposite effect has been observed where unreacted particles act as point defects and thus lower the mechanical strength. In 100%GW S, the Si/Al molar ratio is closer to 100, due to the very low Al-content in the glass wool waste while MK S has a Si/Al ratio of 7.7. Highest strength is achieved for the MK S which contains 60% GW and 40% MK Suggesting that the metakaolin has a significant role in the stabilization of the structure. Metakaolin as raw material contains 27 times more Al than GW raw material. A ratio closer to 1.90, which has shown to be optimum for geopolymers based on metakaolin only, is impossible to achieve in this study without the addition of Al alone. Additionally, 90%GW S, 80%GW S and 70%GW S have shown indications of containing N-A-S-H which would further explain the significantly weaker strength. For 70%GW S, 80%GW S and 90%GW S, the H_2O/M_2O was closer to 1 compared to 100%GW S which may be a further explanation as to them having slightly higher strength.

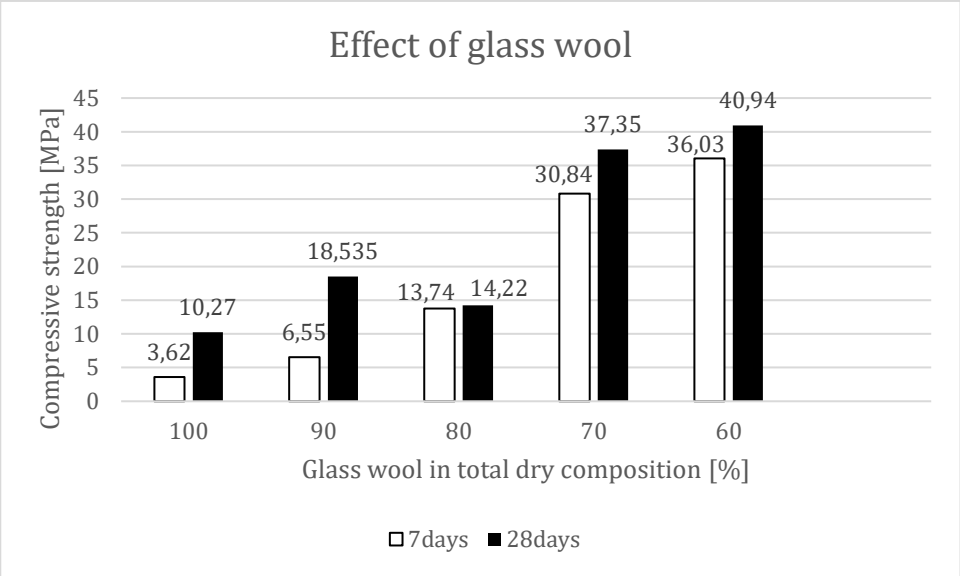

Figure 4.9. The effect of glass wool waste on the compressive strength.

Figure 4.10 and 4.11 presents the effect of Slag1 or Slag2 in the mixture. Compared to the standard sample with 36,03MPa (7 days) and 40,94 MPa (28 days), the addition of Slag1 and Slag2 were not favorable. An increased amount of both types of slags resulted in lower strength. This contradicts the literature studies and indicates that GW and/or metakaolin have a significant role in the strength development. The opposite effect from what literature presents may be due to the slags having

insufficient reaction time as it is the last component to be added to the mixture or differences in the oxide composition. A reaction between Slag1 and water glass resulted in fast hardening, faster than water glass with GW and/or MK.

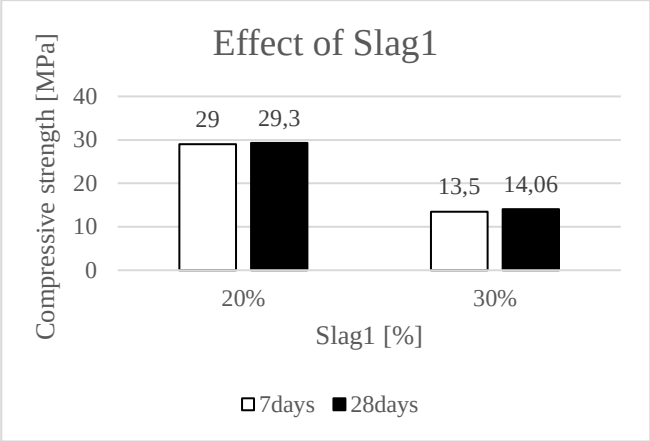

Figure 4.10. Effect of Slag1 on the compressive strength.

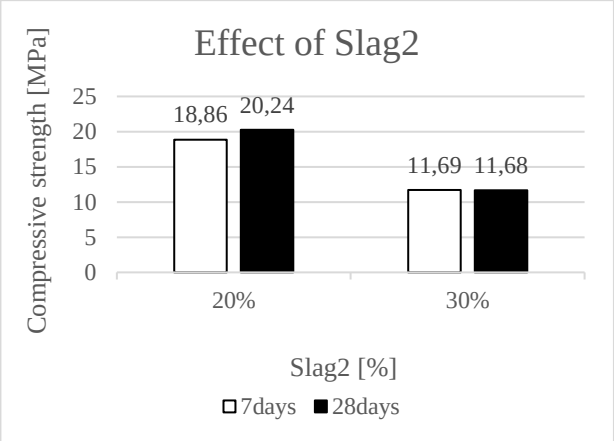

Figure 4.11. Effect of Slag2 on the compressive strength

MK S having little N-A-S-H in comparison to the other samples explains its strength. 100%GW S does not contain the weak gel structure according TGA and ternary diagram. However, deficiency in Al results in no formation of the characteristic tetrahedral network and thus leads to a weaker structure. Presented in are the stress-strain curves of the samples containing MK, Slag1, Slag2 and 100%GW. The latter one having a plastic deformation region due to the less stable structure and higher water content. The other samples show curves that are characteristic for cementitious materials, i.e., brittle nature. The curves for 28 days have a similar shape, but with higher ultimate tensile strength (UTS).

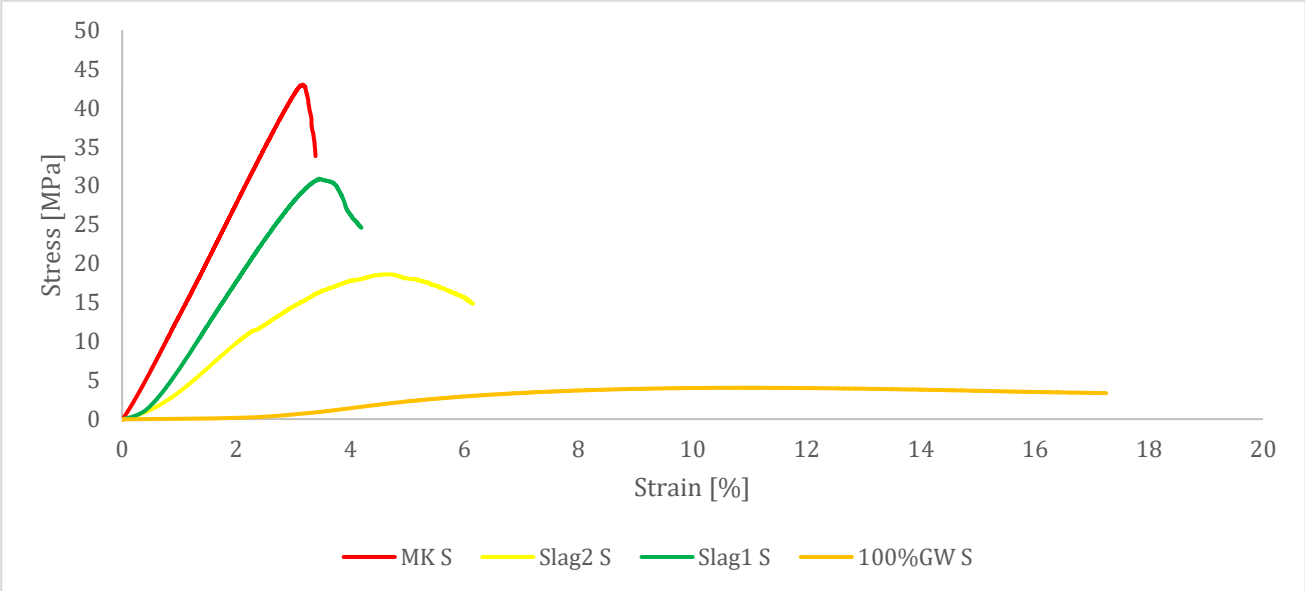

Figure 4.12. Stress-strain curves of samples after 7 days of curing.

Apart from 100%GW S not containing high enough Al to form the characteristic tetrahedral network, the sample also contains higher liquid-to solid ratio (L/S) and also a higher w/b ratio, but same concentration of alkali as the other samples.

The diagram in presents the effect of L/S and w/b on the compressive strength of samples. The compressive strength, alkali concentration and w/b ratio of each measurement are presented in Table 4.1. All samples have been divided into two groups with similar L/S ratios.

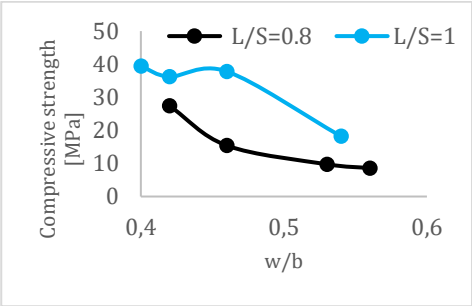

Figure 4.13. Relation between L/S, w/b, alkali concentration and compressive strength

Table 4.2. Relation between L/S, w/b, alkali concentration and compressive strength

L/S=0.8			L/S=1.0		
w/b	Compressive strength [MPa]	Alkali concentration in total liquid amount [%]	w/b	Compressive strength [MPa]	Alkali concentration in total liquid amount [%]
0.42	27.42	35	0.42	36.24	40
0.46	15.41	30	0.46	37.81	40
0.53	9.76	26	0.54	18.20	29
0.56	8.59	23	0.40	39.42	42

Effect of ratios can be looked at individually. However, there is difficulty in varying only one parameter at the time due to multiple parameters being correlated. A higher w/b ratio results in an exponential decrease in strength. This is due to that water does not take part in the build-up of the structure as in traditional OPC where hydrates constitute a big part of the structure. The w/b ratio is related to the concentration of alkali in the liquid. A higher degree of dilution leads to a higher w/b ratio. Comparing the same w/b over the groups, it can be observed that there is a difference in strength, but also a difference in alkali concentration. However, comparing samples with similar alkali concentrations it can be observed that they differ less. This indicates that the alkali concentration may have a more significant role than w/b and L/S. Based on the role of alkali concentration, the difference in strength between MK S, 100%GW S, Slag1 S, Slag2 S thus mainly lies in the elemental composition of the constituting dry components.

4.6 Optical microscopy

Bulk material of the samples showed multiple particles, with the most distinct being the white particles presented in Figure 4.14. Based on the XRD and TGA analysis, the white regions are believed to be a combination of unreacted metakaolin and residual paint from the GW raw material. Unreacted particles can act as solid precipitation and upon subjected to force lead to decreased strength of the material. The exact effect of the dried paint is unknown.

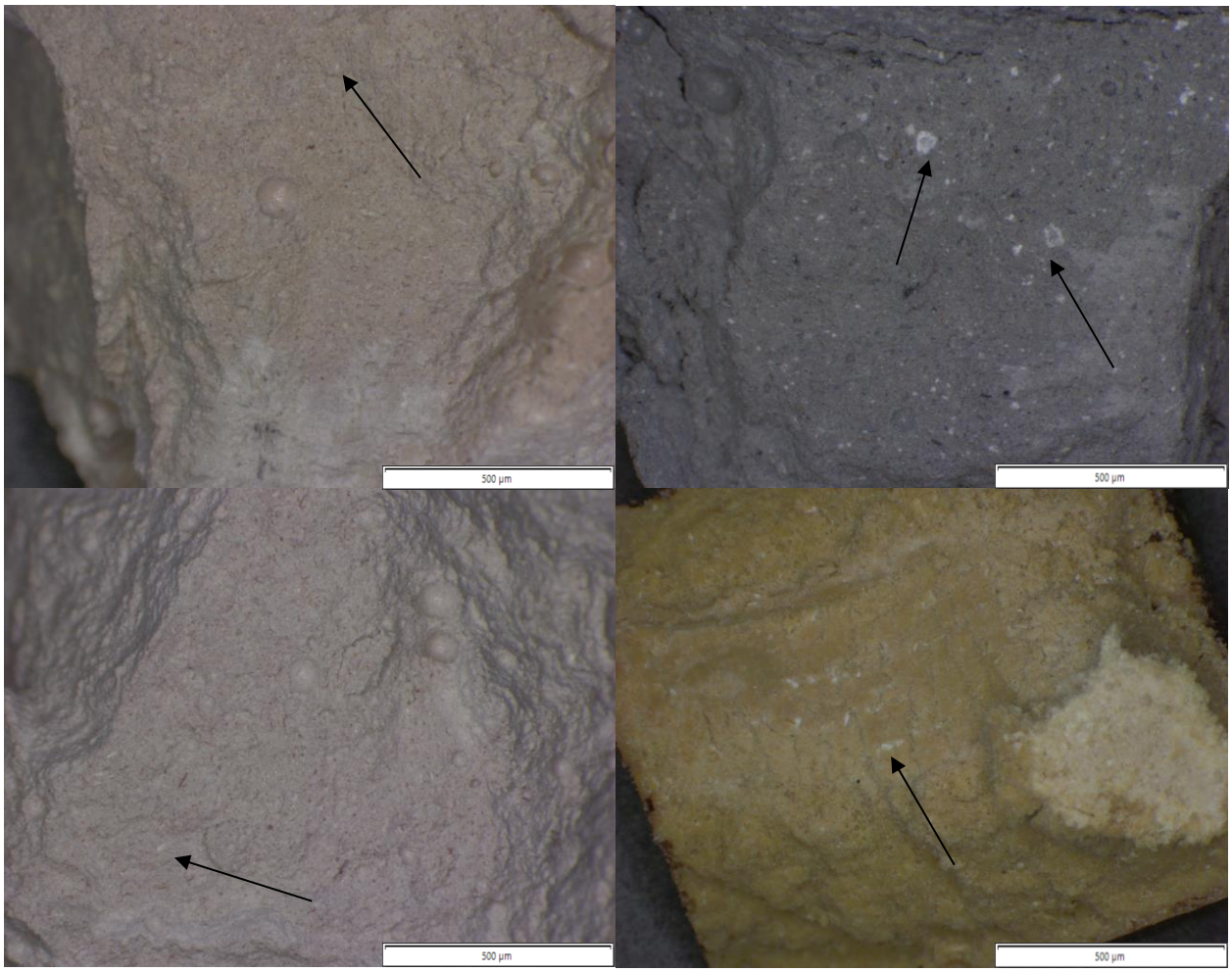

Figure 4.14. MK S (upper left), Slag2 S (upper right), Slag1 S (bottom left), 100% GW S (bottom right)

5 Conclusion

Samples cured at lower temperatures have displayed good strength development, with RT curing being comparable to curing at 40 °C and 60°C. The time could be decreased from 24h to 4h with minor differences in strength at 60 °C. Curing at 40 °C has presented the highest compressive strength in this study. However, generally longer curing times have displayed good strength development with time regardless of temperature.

The compressive strength shows a declining trend upon higher GW content and 60% GW with 40% MK have proven to remain the best composition. Slag1 and Slag2 have a negative effect on the compressive strength of the material. This is likely attributed to the formation of N-A-S-H and C-(N)-A-S-H, and the argument is supported by the results from XRD and TGA analysis. Results from XRD and microscopy indicate the presence of unreacted metakaolin and residual paint which can act as point defects in the microstructure. The alkali concentration in the paste has shown indications to be more significant than w/b and L/S. All samples except for those containing low Al content and low alkali concentration have good strength development and could be used in future applications where higher strengths are required.

Samples in this study are not stoichiometric geopolymers as the ratios between constituting elements are not stoichiometric. There are still residual elements after reaction, including unreacted metakaolin. Lower Si/Al molar ratios, than those in the studied materials, are difficult to achieve with high glass wool content as the raw material contains a low percentage of Al. The true classification (GP or AAM) of the formed materials will vary depending on the different compositions. Those containing low calcium content and a composition outside the regions in which hydrates are formed can still be considered geopolymers as long as there is polycondensation reactions which forms a tetrahedral network with alternating Al and Si. However, an additional characterization technique is required to confirm the presence of gels.

6 Future work

This thesis has compared incorporation of different additives in order to study their effect on formed phases and final properties. Set parameters including 60% GW and 58.3 wt% water were used to determine the differences. The effect of water and alkali concentration have slightly been looked into for samples containing 60% GW and 40% MK. Therefore, it would be interesting to investigate their effect on other compositions. Additionally, to investigate a wider range of alkali concentration and w/b based on the optimum curing parameters obtained from this study. Analysis of samples using FTIR and/or SEM may further be used to confirm the presence of different phases discussed in this study.

Leaching of elements and the effect of heavy metal from the glass wool have not been investigated or discussed in this thesis, and would therefore be of interest to investigate. This is to see if they have significant effect on the strength development.

References

[1]. Yliniemi J, Ramaswamy R, Luukkonen T, Laitinen O, de Sousa ÁN, Huuhtanen M, et al. Characterization of mineral wool waste chemical composition, organic resin content and fiber dimensions: Aspects for valorization. Waste Management. 2021;131:323-30.

[2]. Saint-Gobain Group Saint-Gobainn.d. [cited 2022 10 May]. Available from: https://www.saint-gobain.com/en/group.

[3]. Om Ecophon Ecophon: Ecophon; [cited 2022 May 10]. Available from: https://www.ecophon.com/sv/about-ecophon/.

[4]. Britannica. concrete. Britannica2021.

[5]. Lead C. Grade Of Concrete And Their Uses - Concrete Mix Ratio Civil Leadn.d. [cited 2022 April 15]. Available from: https://www.civillead.com/concrete-mix-ratio-for-various-grade-of-concrete/.

[6]. Aïtcin PC. 3 - Portland cement. In: Aïtcin P-C, Flatt RJ, editors. Science and Technology of Concrete Admixtures: Woodhead Publishing; 2016. p. 27-51.

[7]. PCA. How Cement is Made cement.org: Portland Cement Association; n.d. [cited 2022 April 25]. Available from: https://www.cement.org/cement-concrete/how-cement-is-made.

[8]. Habert G. 1 - Environmental impact of Portland cement production. In: Pacheco-Torgal F, Jalali S, Labrincha J, John VM, editors. Eco-Efficient Concrete: Woodhead Publishing; 2013. p. 3-25.

[9]. Davidovits J. 30 Years of Successes and Failures in Geopolymer Applications. Market Trends and Potential Breakthroughs. . Geopolymer 2002 Conference; 28-29 October; Melbournce, Australia. www.geopolymer.org2002.

[10]. Weil M, Dombrowski K, Buchwald A. 10 - Life-cycle analysis of geopolymers. In: Provis JL, van Deventer JSJ, editors. Geopolymers: Woodhead Publishing; 2009. p. 194-210.

[11]. What is a geopolymer? Introduction Geopolymer Institute: Geopolymer Institute; 2006 [cited 2022 4 April]. Available from: https://www.geopolymer.org/science/introduction/.

[12]. Joseph D. Geopolymer Chemistry & Applications. Joseph D, editor: Institute Géopolymère 2020. 674 p.

[13]. Janošević N, Snezana D-V, Toplicic-Curcic G, Karamarkovic J. Properties of geopolymers. Facta universitatis - series Architecture and Civil Engineering. 2018;16:45-56.

[14]. Gellert R. 8 - Inorganic mineral materials for insulation in buildings **This chapter is dedicated to Dr Walter F. Cammerer on the occasion of his 90th birthday. In: Hall MR, editor. Materials for Energy Efficiency and Thermal Comfort in Buildings: Woodhead Publishing; 2010. p. 193-228.

[15]. Yliniemi J, Kinnunen P, Karinkanta P, Illikainen M. Utilization of Mineral Wools as Alkali-Activated Material Precursor. Materials. 2016;9:312.

[16]. Rasekh H, Joshaghani A, Jahandari S, Aslani F, Ghodrat M. 2 - Rheology and workability of SCC. In: Siddique R, editor. Self-Compacting Concrete: Materials, Properties and Applications: Woodhead Publishing; 2020. p. 31-63.

[17]. Pozzolana. Merriam-Webstern.d. Pozzolana.

[18]. Thankam G, Renganathan N. Ideal supplementary cementing material – Metakaolin: A review. International Review of Applied Sciences and Engineering. 2020;11.

[19]. Ghassemi M, Andersen PK, Ghassemi A, Chianelli RR. Hazardous Waste from Fossil Fuels. In: Cleveland CJ, editor. Encyclopedia of Energy. New York: Elsevier; 2004. p. 119-31.

[20]. El-Chabib H. 11 - Properties of SCC with supplementary cementing materials. In: Siddique R, editor. Self-Compacting Concrete: Materials, Properties and Applications: Woodhead Publishing; 2020. p. 283-308.

[21]. Saludung A, Ogawa Y, Kawai K. Microstructure and mechanical properties of FA/GGBS-based geopolymer. MATEC Web of Conferences. 2018;195:01013.

[22]. Bellum RR, Muniraj K, Madduru SRC. Exploration of mechanical and durability characteristics of fly ash-GGBFS based green geopolymer concrete. SN Applied Sciences. 2020;2(5):919.

[23]. Duxson P, Provis JL, Lukey GC, Mallicoat SW, Kriven WM, van Deventer JSJ. Understanding the relationship between geopolymer composition, microstructure and mechanical properties. Colloids and Surfaces A: Physicochemical and Engineering Aspects. 2005;269(1):47-58.
[24]. He P, Wang M, Fu S, Jia D, Yan S, Yuan J, et al. Effects of Si/Al ratio on the structure and properties of metakaolin based geopolymer. Ceramics International. 2016;42(13):14416-22.
[25]. Abdullah MMAB, Kamarudin H, Abdulkareem OA, Ruzaidi C, Razak R. The effect of alkaline activator ratio on the compressive strength of fly ash-based geopolymers. The effect of alkaline activator ratio on the compressive strength of fly ash-based geopolymers. 2011;5:1916-022.
[26]. Luan C, Shi X, Zhang K, Utashev N, Yang F, Dai J, et al. A mix design method of fly ash geopolymer concrete based on factors analysis. Construction and Building Materials. 2021;272:121612.
[27]. Komnitsas K, Zaharaki D. Geopolymerisation: A Review and Prospects for the Minerals Industry. Minerals Engineering. 2007;20:1261-77.
[28]. Phair JW, Van Deventer JSJ. Effect of the silicate activator pH on the microstructural characteristics of waste-based geopolymers. International Journal of Mineral Processing. 2002;66(1):121-43.
[29]. Davidovits J. Geopolymer for newcomers by Prof Dr Joseph DAVIDOVITS; France2021.
[30]. Panagiotopoulou C, Kontori E, Perraki T, Kakali G. Dissolution of Aluminosilicate Minerals and by-Products in Alkaline Media. Journal of Materials Science - J MATER SCI. 2007;42:2967-73.
[31]. Institute G. geopolymer.org; 2021.
[32]. van Dokkum HP, Hulskotte JHJ, Kramer KJM, Wilmot J. Emission, Fate and Effects of Soluble Silicates (Waterglass) in the Aquatic Environment. Environmental Science & Technology. 2004;38(2):515-21.
[33]. Andreola F, Barbieri L, Lancellotti I. The Environmental Friendly Route to Obtain Sodium Silicate Solution from Rice Husk Ash: A Comparative Study with Commercial Silicates Deflocculating Agents. Waste and Biomass Valorization. 2020.
[34]. Muñiz-Villarreal MS, Manzano-Ramírez A, Sampieri-Bulbarela S, Gasca-Tirado JR, Reyes-Araiza JL, Rubio-Ávalos JC, et al. The effect of temperature on the geopolymerization process of a metakaolin-based geopolymer. Materials Letters. 2011;65(6):995-8.
[35]. Mo B-h, Zhu H, Cui X-m, He Y, Gong S-y. Effect of curing temperature on geopolymerization of metakaolin-based geopolymers. Applied Clay Science. 2014;99:144-8.
[36]. García-Lodeiro I, Maltseva O, Palomo A, Fernández-Jiménez A. Hybrid alkaline cements. Part I: Fundamentals. Revista Romana de Materiale/ Romanian Journal of Materials. 2012;42:330-5.
[37]. Ralli Z, Pantazopoulou S. State of The Art on Geopolymer Concrete. International Journal of Structural Integrity. 2020.
[38]. Smith609. Blank ternary plot. In: plot Bt, editor. Wikimedia commons2017.
[39]. Harrisson AM. 4 - Constitution and Specification of Portland Cement. In: Hewlett PC, Liska M, editors. Lea's Chemistry of Cement and Concrete (Fifth Edition): Butterworth-Heinemann; 2019. p. 87-155.
[40]. Marchon D, Flatt RJ. 8 - Mechanisms of cement hydration. In: Aïtcin P-C, Flatt RJ, editors. Science and Technology of Concrete Admixtures: Woodhead Publishing; 2016. p. 129-45.
[41]. Cuesta A, Santacruz I, De la Torre AG, Dapiaggi M, Zea-Garcia JD, Aranda MAG. Local structure and Ca/Si ratio in C-S-H gels from hydration of blends of tricalcium silicate and silica fume. Cement and Concrete Research. 2021;143:106405.
[42]. Adesanya E, Ohenoja K, Di Maria A, Kinnunen P, Illikainen M. Alternative alkali-activator from steel-making waste for one-part alkali-activated slag. Journal of Cleaner Production. 2020;274:123020.
[43]. Lemougna PN, Adediran A, Yliniemi J, Luukkonen T, Illikainen M. Effect of organic resin in glass wool waste and curing temperature on the synthesis and properties of alkali-activated pastes. Materials & Design. 2021;212:110287.

[44]. Yliniemi J, Walkley B, Provis JL, Kinnunen P, Illikainen M. Nanostructural evolution of alkali-activated mineral wools. Cement and Concrete Composites. 2020;106:103472.
[45]. Puertas F, Palacios M, Manzano H, Dolado JS, Rico A, Rodríguez J. A model for the C-A-S-H gel formed in alkali-activated slag cements. Journal of the European Ceramic Society. 2011;31(12):2043-56.
[46]. Quartz Mindat.orgn.d. [cited 2022 20 May]. Available from: https://www.mindat.org/min-3337.html.
[47]. Will G, Bellotto M, Parrish W, Hart M. Crystal Structure of Quartz and Magnesium Germinate by Profile Analysis of Synchrotron-Radiation High-Resolution Powder Data. Journal of Applied Crystallography - J APPL CRYST. 1988;21:182-91.
[48]. X-ray diffraction KTH202 [updated Oct 14, 2020; cited 2022 28 april]. Available from: https://www.kth.se/hultgrenlab/our-services/techniques/x-ray-diffraction-1.1018932.
[49]. Dickens B, Brown WE. Crystal structures of CaNa2(CO3)2.5H2O, synthetic gaylussite, and CaNa2(CO3)2.2H2O, synthetic pirssonite. Inorganic Chemistry. 1969;8(10):2093-103.
[50]. Mullite Mindat.orgn.d. [cited 2022 May 13]. Available from: https://www.mindat.org/min-2806.html.
[51]. Angel RJ, Prewitt CT. Crystal structure of mullite: A re-examination of the average structure. American Mineralogist. 1986;71(11-12):1476-82.
[52]. Nepheline Mindat.orgn.d. [cited 2022 May 10]. Available from: https://www.mindat.org/min-2880.html.
[53]. Nepheline n.d. [cited 2022 May 16]. Available from: http://rruff.geo.arizona.edu/AMS/authors/Klein%20G.
[54]. Calcite Mindat.orgn.d. [cited 2022 May 12]. Available from: https://www.mindat.org/min-859.html.
[55]. Wyckoff RWG. The crystal structures of some carbonates of the calcite group. American Journal of Science.317-60.
[56]. Schick C. Calorimetry. Reference Module in Materials Science and Materials Engineering: Elsevier; 2016.
[57]. Singh JP, Verma S. 3 - Raw materials for terry fabrics. In: Singh JP, Verma S, editors. Woven Terry Fabrics: Woodhead Publishing; 2017. p. 19-28.
[58]. Chem538w10grp5. In: Cruve2.PNG S-S, editor. Wikimedia commons2010.
[59]. ARMICRON. Bragg diffraction. In: diffraction.svg B, editor. Wikimedia commons: Wikimedia commons; 2010.
[60]. Britannica TEoE. X-ray diffraction. Britannica. Britannican.d.
[61]. Thermogravimetric analysis (TGA) [Internet]. Chemistry LibreTexts. 2020. Available from: https://chem.libretexts.org/Courses/Franklin_and_Marshall_College/Introduction_to_Materials_Characterization__CHM_412_Collaborative_Text/Thermal_Analysis/Thermogravimetric_analysis_(TGA).
[62]. Merabtene M, Kacimi L, Clastres P. Elaboration of geopolymer binders from poor kaolin and dam sludge waste. Heliyon. 2019;5(6):e01938.
[63]. Lemougna PN, Adediran A, Yliniemi J, Ismailov A, Levanen E, Tanskanen P, et al. Thermal stability of one-part metakaolin geopolymer composites containing high volume of spodumene tailings and glass wool. Cement and Concrete Composites. 2020;114:103792.
[64]. Rosas C, Arredondo-Rea S, Gómez-Soberón J, Almaral J, Corral Higuera R, Chinchillas-Chinchillas MJ, et al. Experimental study of XRD, FTIR and TGA techniques in geopolymeric materials. International Journal for Housing Science and Its Applications. 2014;4:221-7.
[65]. Microscopy reference card University of Readingn.d. [cited 2022 May 15]. Available from: https://www.reading.ac.uk/web/files/ta/Microscopy_(CfAM)_reference_card.pdf.
[66]. Ingham JP. 1 - Introduction. In: Ingham JP, editor. Geomaterials Under the Microscope. Boston: Academic Press; 2013. p. 7-20.

[67]. L G, Sheethal K, Puttiah PK, M t P. Development of High Strength Geopolymer Concrete using Low Molarity Naoh. International Journal of Engineering Research and. 2015;V4.

APPENDIX A

Appendix A presents individual XRD spectra of each sample and raw material.

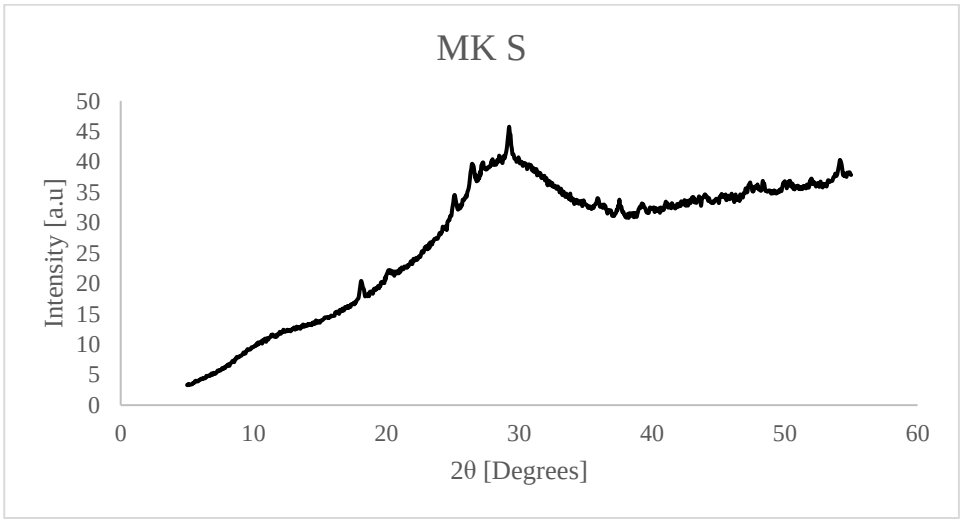

Figure A 1. XRD spectra of MK S

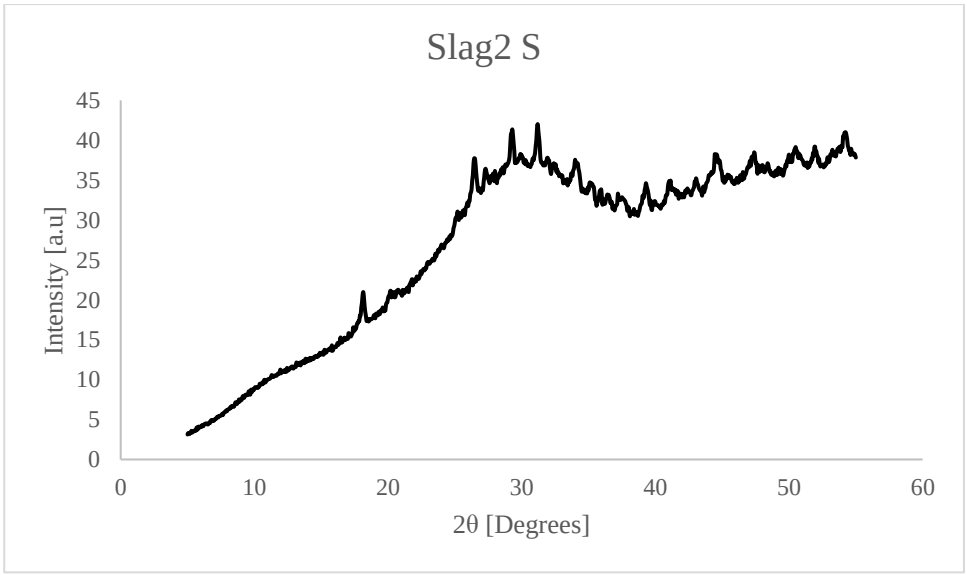

Figure A 2. XRD spectra of Slag2 S

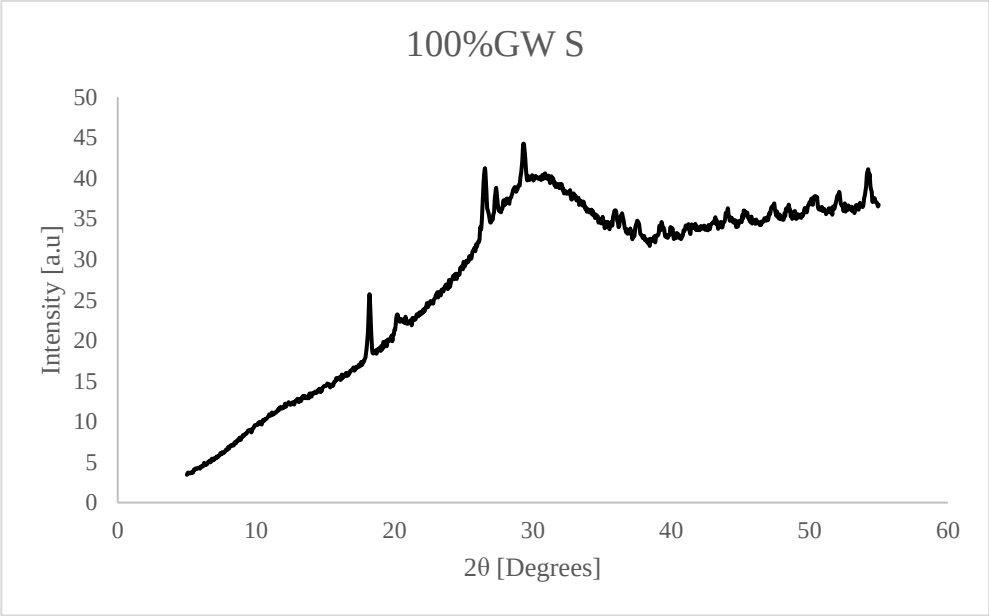

Figure A 3. XRD spectra of 100%GW S

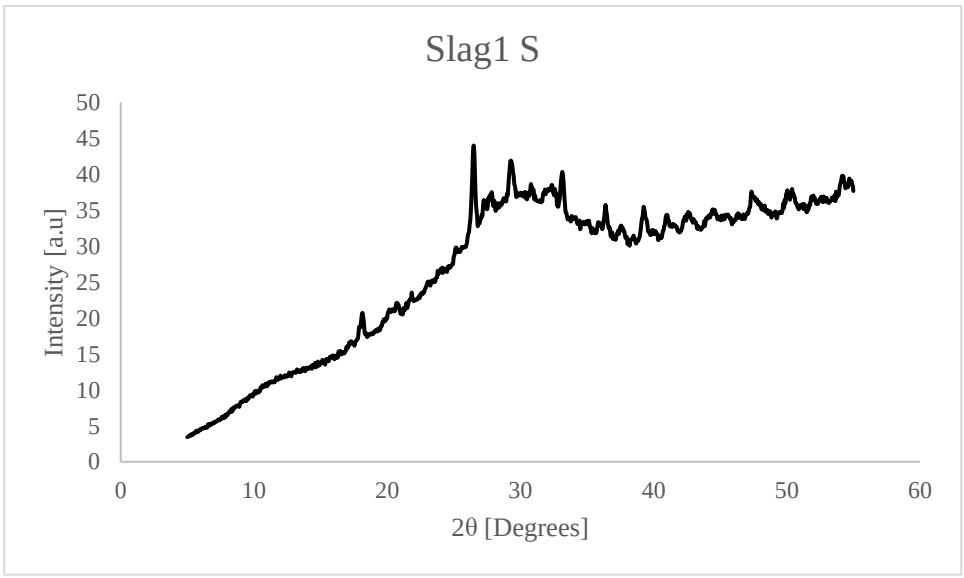

Figure A 4. XRD spectra of Slag1 S

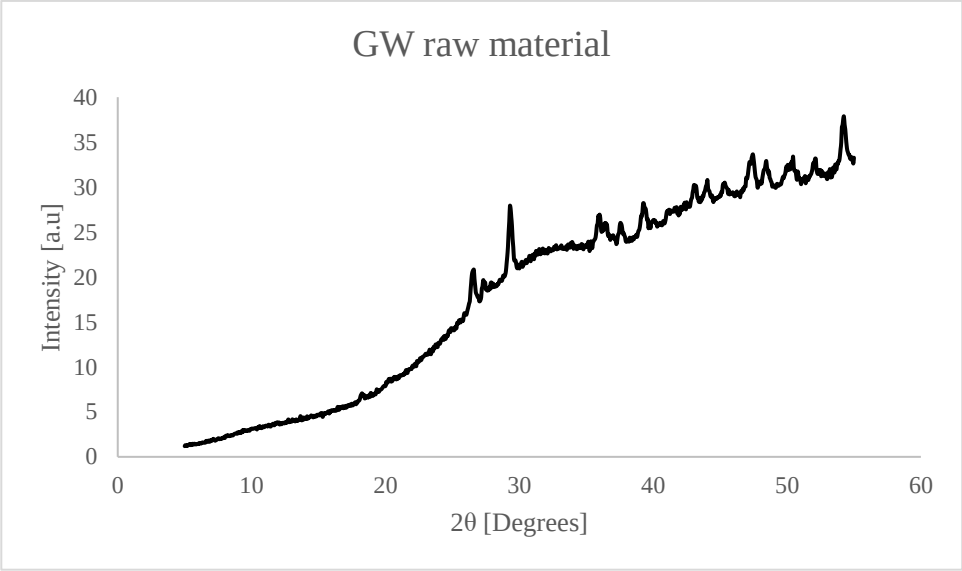

Figure A 5. XRD spectra of GW raw material

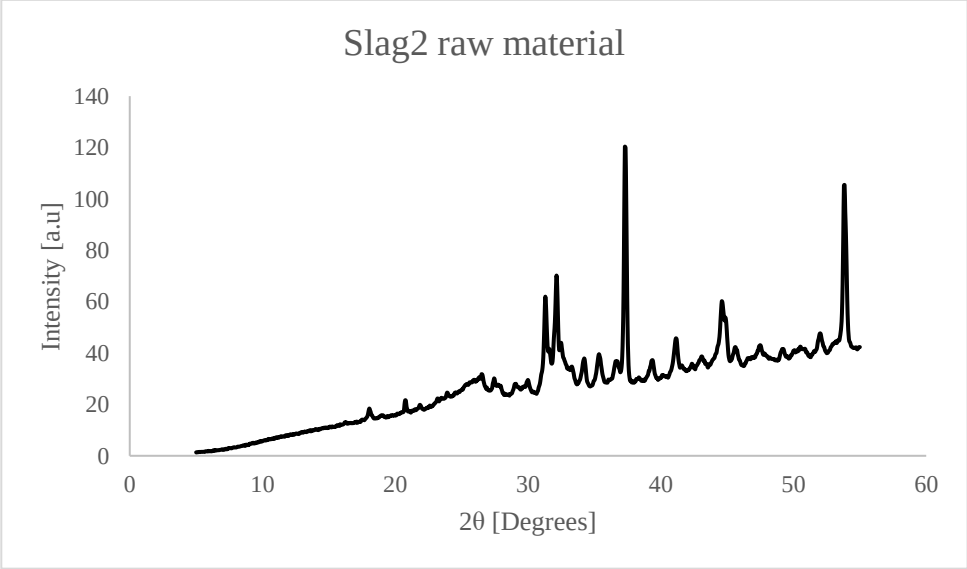

Figure A 6. XRD spectra of Slag2 raw material

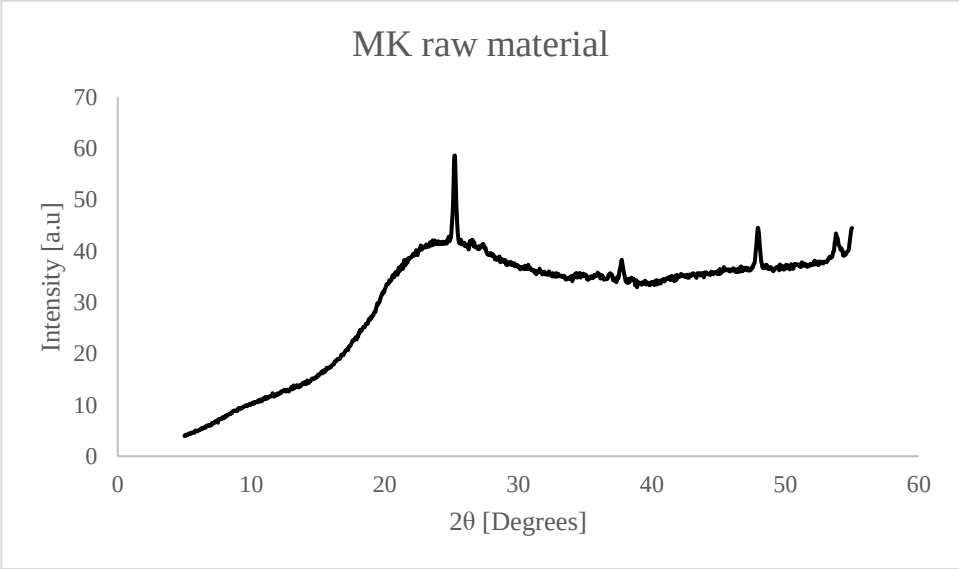

Figure A 7. XRD spectra of MK raw material

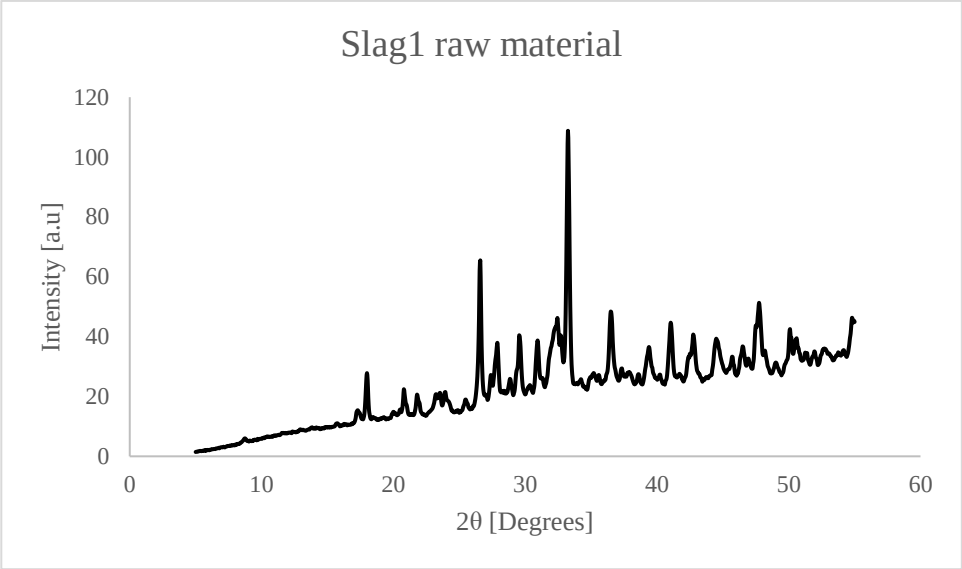

Figure A 8. XRD spectra of Slag1 raw material

APPENDIX B

Appendix B presents TGA and DTG curves of samples containing GW, MK, Slag2 and Slag1.

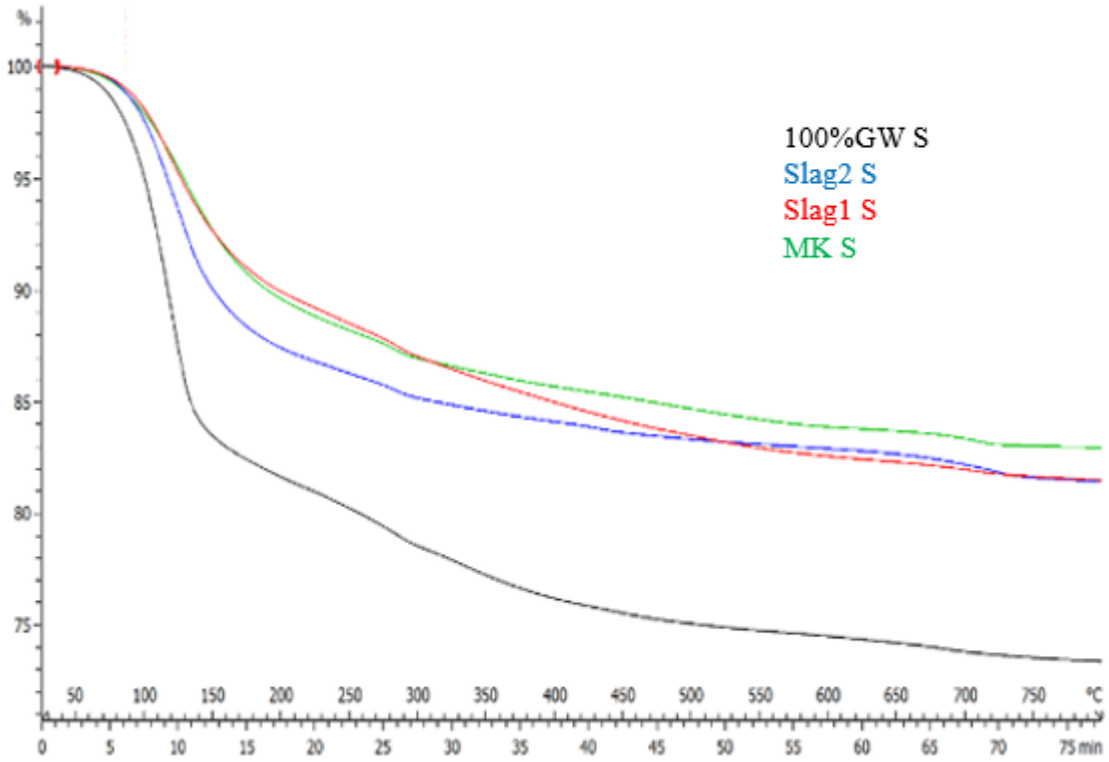

Figure B 1. TGA of 100%GW S, 20%Slag1 S, 20%Slag2 S and MK S

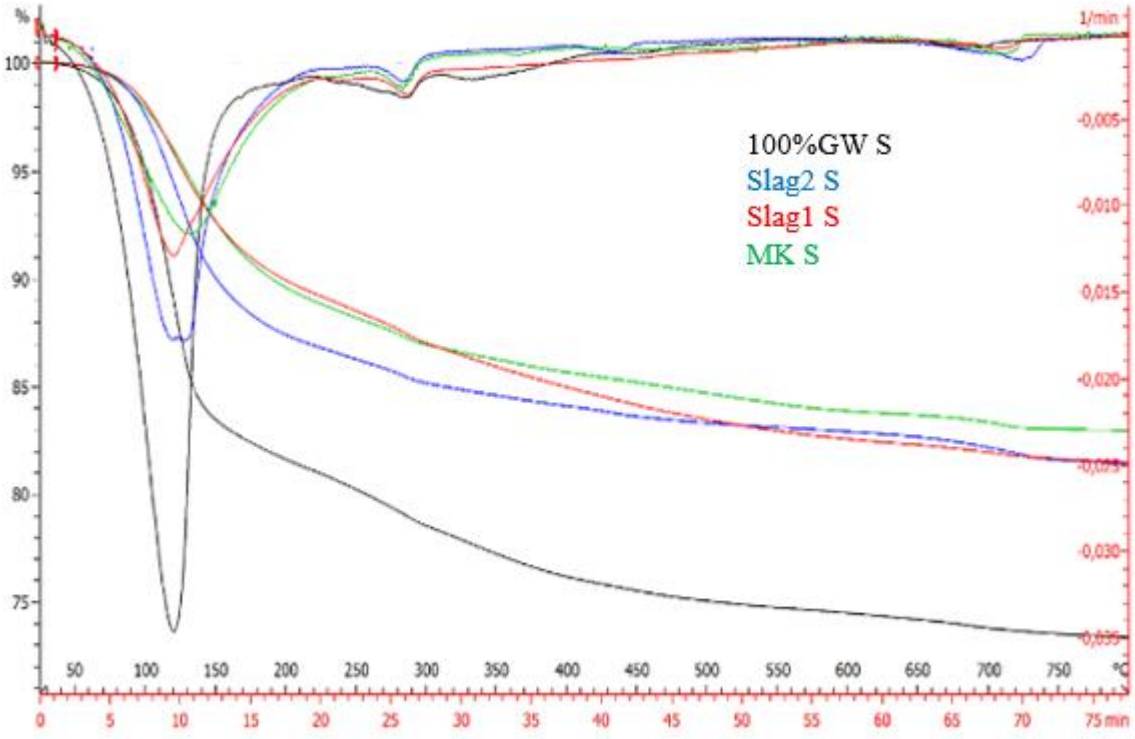

Figure B 2. TGA and DTG of 100%GW S, 20%Slag1 S, 20%Slag2 S and MK S

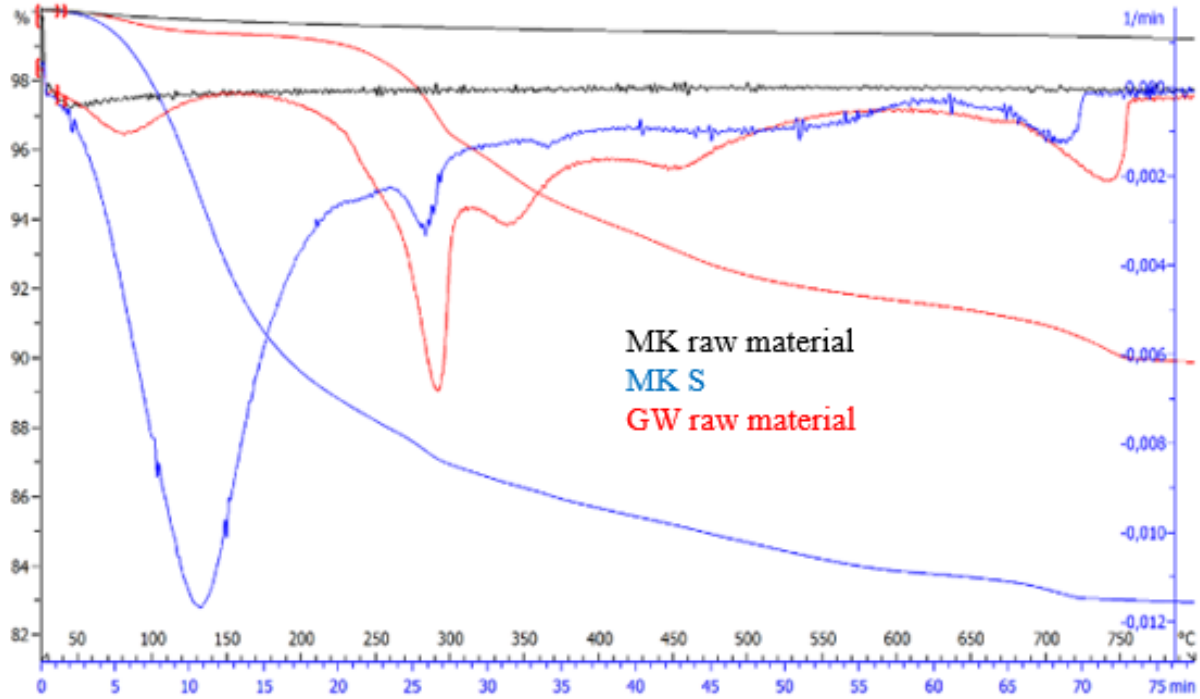

Figure B 3. TGA and DTG of MK S and its raw materials

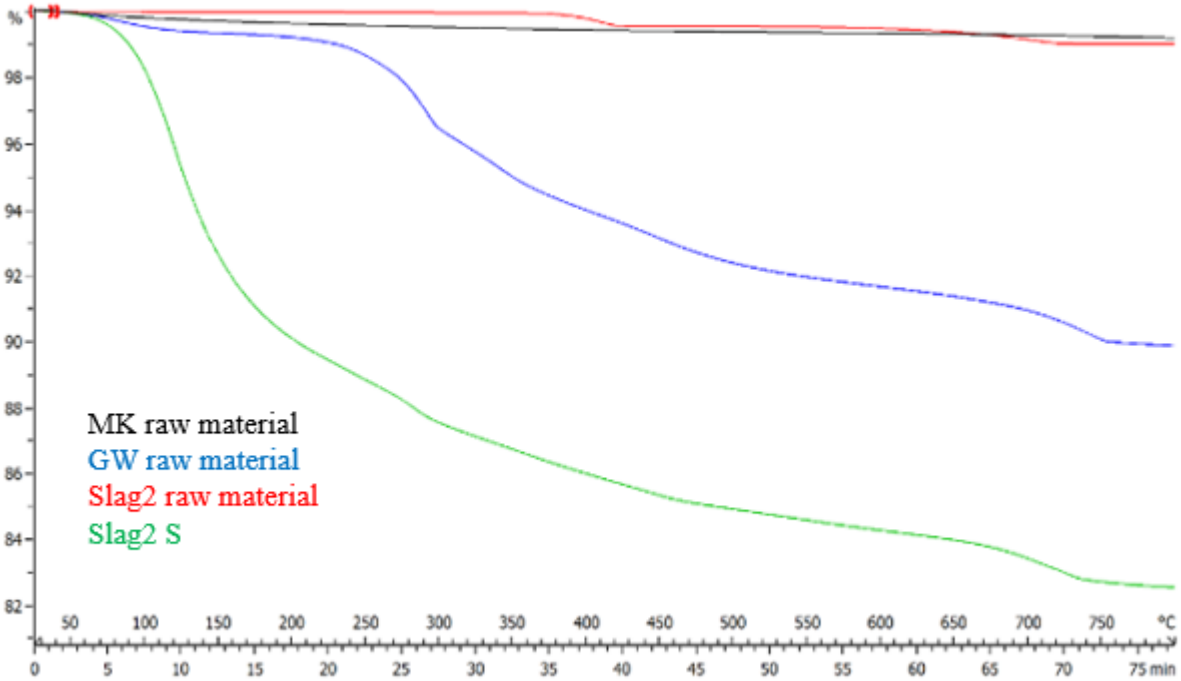

Figure B 4. TGA of Slag2 S and its raw materials

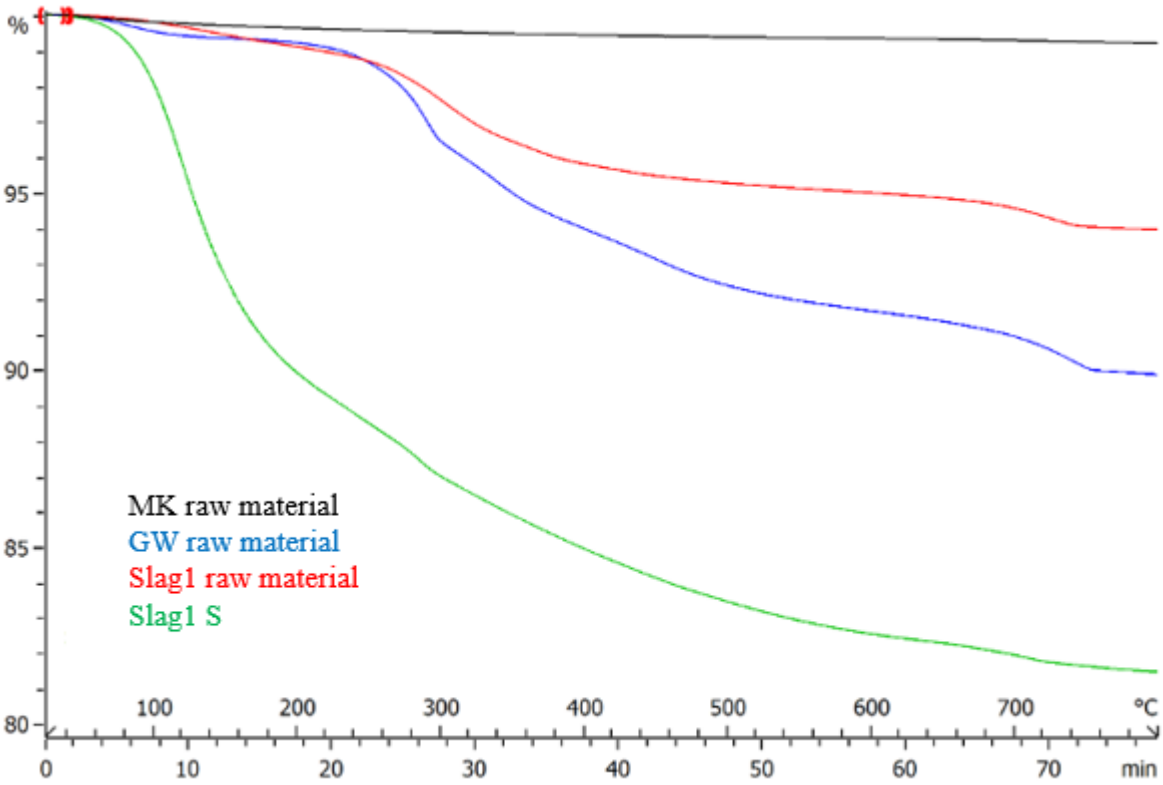

Figure B 5. TGA of Slag1 S and its raw materials

DEPARTMENT OF CHEMISTRY AND CHEMICAL ENGINEERING

CHALMERS UNIVERSITY OF TECHNOLOGY
Gothenburg, Sweden 20xx
www.chalmers.se

CHALMERS
UNIVERSITY OF TECHNOLOGY